行政院原子能委員會

委託研究計畫研究報告

創新加壓型固態氧化物燃料電池設計測試及模擬分析 II

Experimental and Numerical Simulation of Innovative Pressurized-Assembling Designs for Solid Oxide Fuel Cell II

計畫編號：**1002001INER054**

受委託機關(構)：國立中央大學

計畫主持人：施聖洋

聯絡電話：**03-4267327**

E-mail address: sshy@ncu.edu.tw

核研所聯絡人員：羅世坤

報告日期：**100** 年 **12** 月 **28** 日

目　錄

中文摘要

本計畫之目標為利用實驗測試和數值模擬方法，研究加壓效應對固態氧化物燃料電池(SOFC)性能之影響。我們成功建立一套創新加壓型 SOFC 之實驗測試平台，並已經進行一系列加壓條件下之單電池堆性能測試與模擬分析。本計畫所得之結果，應對未來發展高效率 SOFC 與氣渦輪機發電系統之整合技術有所幫助。本計畫產出之成果有五項：(1)完成加壓型 SOFC 國際相關文獻之彙整與分析工作；(2)完成加壓型 SOFC 性能測試平台之建置，並已執行一系列 SOFC 單電池堆於不同加壓條件下(1 ~ 5 大氣壓)之性能測試和阻抗頻譜量測；(3)已建立加壓型 SOFC 單電池堆三維化學反應流數值模型，配合實驗執行相關之數值運算，分析單電池堆內部之溫度與濃度分佈；(4)利用已建立的高溫密封材料洩漏率測試平台，完成新型壓縮式密封材料於高溫條件下之洩漏率測試，並提出優化的密封材料製程參數;(5) 2011 年發表一篇國際 SCI 期刊論文(*J. Power Sources*)和四篇國際與國內會議論文。

關鍵字：加壓型平板式固態氧化物燃料電池、電池堆、壓力效應、電池性能測試平台

英文摘要

This project aims to experimentally and numerically study the effect of pressurization on the cell performance of solid oxide fuel cells (SOFC). Thus, we have established an innovative platform to measure the cell performance of the single-cell stack operated at elevated pressure conditions. The results should be of help in the future development of the high-efficiency hybrid power source that combines SOFC and gas turbine. The followings are the project output including five items. (1) The completion of pressurized SOFC literatures review. (2) A platform for the testing of pressurized SOFC single-cell stacks has been established. Therefore, the effect of pressurization on the cell performance of SOFC was quantitatively investigated by measuring the power-generating characteristics and the electrochemical impedance spectra of single-cell stacks under different elevated pressure conditions (1 ~ 5 atm). (3) A 3-dimentional numerical model was also established to simulate the aforementioned pressurized experiments and then used to predict the temperature and concentration fields in pressurized SOFC. (4) We have measured the leakage rates of the novel sealing material under high temperature conditions by using an established high-temperature platform. Based on our results, an optimal combination of different processing parameters for manufacturing a new compressive sealant with a reasonable good tightness is proposed. (5) We have published one paper in *J. Power Sources* (SCI) and four conference papers.

Key words: planar solid oxide fuel cell, stack, pressurized, cell testing platform

壹、計畫緣起與目的

加壓型固態氧化物燃料電池(SOFC)可與淨煤技術及微氣渦輪機發電技術結合，被先進國家認定為未來定置型發電系統的重要選項。本計畫配合核能研究所「新能源技術之發展與應用」計畫項下之「燃料電池發電」，針對加壓型 SOFC 的組裝技術及性能特性進行研發。本計畫主要推動的研究工作有三項：(1)彙整加壓式 SOFC 的相關文獻回顧；(2)研究分析加壓型 SOFC 之性能；(3)研發高氣密性且低成本之新型壓縮式密封材料，所獲得之成果可有助於核研所合作夥伴達成上位計畫之目標。

一、計畫緣起

我國近年來的經濟持續成長，因此能源的需求仍隨之快速增長。在面對國際間積極推動節能與溫室氣體減量的雙重壓力下，我們更應積極發展前瞻的能源利用技術，將珍貴的初級能源高效率地轉換成低污染的動力或電能。燃料電池能將燃料的化學能直接轉換為電能，且副產物只有水，是一種高效率且對環境十分友善的能源載具。有別於其他再生能源技術，例如風力、太陽能或是潮汐發電等，燃料電池不易受氣候影響，可穩定提供電能，符合我國追求能源安全之目標，是一種相當值得投入研發的能源利用技術。

燃料電池的演進歷史約已超過 150 年的時間，目前已有許多不同種類的燃料電池被開發，其中 SOFC 具有高能源轉換效率、燃料使用多元化以及低污染物排放等缺點，能夠兼具國家能源安全、經濟發展以及環境永續之需求，相當具有發展優勢。近年來，SOFC 結合氣渦輪機(gas turbine, GT)之複合式發電系統相當受到矚目，因為 GT 能有效再利用 SOFC 尾氣所含的燃氣與廢熱，這不僅能提高發電系統的燃料使用率，還能輸出更多的電能，將其發展為分散式定置型電力供應系統，將可減少集中式供電系統在電力傳輸過程中之能量損耗[1]。然而，GT 須在較高壓的條件下操作，方能發揮其性能與效率，但目前的 SOFC 技術研發則多以常壓條件為主，如何讓 SOFC 能在高壓環境下穩定操作，並使其尾氣可與 GT 的操作條件契合，將是複合式發電技術能否發展成功的關鍵技術。

我國核能研究所自 2003 年起開始著手研發平板式 SOFC 之發電技術，至今已獲得相當豐富的研究成果，含成功組裝與測試 kW 等級 SOFC 電池堆，已可自行研製陽極支撐或金屬支撐電池基板(positive electrode-electrolyte-negative electrode, PEN)，設計製作燃料電池平衡系統(balance-of- plant)相關組件，並已建立用於預測電池性能與整體系統發電效率之數值模式[2-5]。而為了能將上述之成果的應用層面進一步擴展至 SOFC-GT 的複合式發電系統，核研所目前

亦開始針對加壓式 SOFC 以及金屬支撐 PEN 等具前瞻性之議題進行研究。因此，本計畫全力配合核研所的 SOFC 研發策略，建立加壓型 SOFC 之研究能量，期能藉由電池性能量測、阻抗頻譜分析以及數值模擬等基礎學理層面之研究方法，研究加壓型 SOFC 之性能特性。此外，我們並建立一套高溫高壓的氣體洩漏率測試平台，測試不同的密封料與組裝技術在加壓型 SOFC 操作環境之洩漏率。本計畫所獲得之相關重要資料，應對於核研所未來擬進行之複合式發電系統研發有實質的幫助。

二、計畫目的

本計畫最主要目的是研究加壓型 SOFC 性能特性，以及設計相關之組裝技術，並歸納相關之研究數據資料，讓核研所之合作夥伴有可供參考之資料。本計畫所探討的兩大問題分述如下：

(一) 研究加壓型 SOFC 及其流場均勻度效應對電池性能之影響

近年來，研發 SOFC-GT 複合式發電系統的相關研究相當受到矚目。然而，如何讓 SOFC 在高壓環境下穩定操作，使其尾氣可較容易與 GT 的操作條件契合，卻是仍待克服的關鍵技術。目前多種不同的電池堆設計中，美國 Siemens-Westinghouse 所開發的 tubular SOFC 以及 Rolls-Royce 所提出的 integrated planar SOFC，因其氣密

性較佳，是兩種目前最常被應用於加壓型 SOFC 的設計[6,7]。而傳統的平板式 SOFC，如核研所目前研發中的雙進口/單出口設計，則較少相關文獻可供參考。為此，本計畫進行了完整的文獻回顧與分析，以了解壓力效應對於電池性能以及電池操作壽命的影響。此外，本計畫延續上年度之研究工作，改良已具雛型的加壓型 SOFC 性能測試平台，提升其穩定度與可靠度，並建立標準化之加壓實驗流程。利用此平台與標準實驗流程，我們已可執行一系列的加壓型 SOFC 性能測試。是故，本計畫結合實驗與數值模擬方法，研究流場均勻度效應對加壓型 SOFC 單電池堆性能之影響。

(二) 開發新型低成本高氣密性之密封材料

開發低成本且高氣密性的前瞻密封材料，是 SOFC 商品化的關鍵技術之一。目前已被開發的 SOFC 密封材料可分為壓縮式密封材料(Compressive seals)和剛性密封材(Rigid seals)兩種[8]，前者的氣密效果雖然略優於前者，但卻非常不利於元件的更換，故其發展性受到相當大的限制。為了評估不同壓縮式密封材料應用於加壓型SOFC之可行性，本計畫首先建立一套氣體洩漏率實驗平台，以測試不同壓縮式密封材料，如雲母和銀線，於高溫環境下之洩漏率(R_l)。此外，本計畫利用氣相式二氧化矽(fumed silica)和陶瓷纖維，製作可適用於SOFC 且成本低的新型壓縮式密封材料。我們採用與 Le et al.[9]相同

的製程，但深入研究不同製程參數，如氣相式二氧化矽溶液濃度、烘烤溫度(T_{dry})、預壓壓力(p_c)等，對新型壓縮式密封材料氣密性之影響，進而找出優化的製程參數。

貳、文獻回顧

SOFC 與 GT 的結合發電系統，可有效地提升系統整體的發電效率以及燃料使用率，是一種兼具經濟、環保與高效率的發電技術。若以 SOFC 電池堆的操作壓力對 SOFC-GT 複合發電系統進行分類，則有加壓式與常壓式兩種[10]。美國 Siemens-Westinghouse 是發展 SOFC-GT 複合發電系統的先驅，他們自 2000 年起，已建立許多不同發電規模，且以管狀 SOFC 電池堆為基礎的複合發電系統。在 Siemens-Westinghouse 目前已獲得的研究數據中，加壓式的複合發電系統可有較高的發電效率，以可將 SOFC 操作於約 7 bar 條件下的複合發電系統為例，當系統的發電規模為 2 百萬瓦以及 2 千萬瓦時，相對應的發電效率分別可達 60%與 70%，說明了加壓式複合發電系統的發展潛力[11]。正因加壓式 SOFC-GT 複合發電系統有如此優異的性能，相關的研發工作正逐漸開始蓬勃發展，其中一部份的研究是以數值模擬或熱力學分析的方式，預測加壓式 SOFC 與 GT 的優化操作參數，如文獻[12,13]。而另一部份的研究則是分以美國 Siemens-Westinghouse 公司所建立的示範發電系統為例[1]，常壓型

SOFC-GT 系統中加壓的高溫空氣會經過熱交換器，先驅動 GT，然後再通入 SOFC。加壓型 SOFC-GT 系統則是將高壓高溫空氣先通入 SOFC，之後的尾氣再用來驅動 GT。由於 GT 的進口溫度會隨著壓力比增加而降低，故若採用高壓力比的 GT 設計，則加壓型 SOFC 將可有效改善進口溫度降低的問題，進而提升整體效率。

數值模擬方面，Ni et al. [14]以 Bulter-Volmer equation、Fick's law 以及 Ohmic law 建立一維的 SOFC 數值模式，並預測可具最佳電池性能的優化電極微結構以及優化操作條件。此研究所探討的操作壓力範圍為 0.5 bar ~ 5 bar，其結果顯示增加操作壓力有助於提升反應物的擴散率，而這不僅使電極觸媒的表面可完全與反應物接觸，降低活化極化，同時也可加快多孔電極內反應物與生成物的交換，進而抑制濃度極化現象。Patcharavorachot et al. [15]進一步修改 Ni et al. [14]的數值模式，將用於描述 SOFC 活化極化的 Bulter-Volmer equation 由原來的線性表示法改為非線性表示法，即交換電流密度(exchange current density)需由電化學反應率之指數前置因子(pre-exponential factor)以及反應物活化能(activation energy)求得，而非一常數。經過修改後的數值模擬結果發現[15]，增加 SOFC 的操作壓力可明顯抑制濃度極化，但對活化極化的影響則相當不明顯。Bo et al. [16]不僅建立與前二者相似之數值模式，探討壓力效應對電

池性能極化現象的影響，也利用 Aspen Plus 軟體分析 SOFC 在高壓條件下之發電效率。Bo et al. [16]的結果與 Ni et al. [14]相同，歸納出陽極的活化過電位及濃度過電位，隨操作壓力增加而下降原因：(1)操作壓力增加，則氣體濃度增加；(2)壓力增加，則氣體莫耳擴散率增加，因此有較低的濃度過電位；(3)壓力增加，在燃氣高莫耳濃度環境下，多孔性電極變得活躍，因此有較低活化過電位。但若要增加 SOFC 的操作壓力，則系統需要額外裝置一壓縮機，而壓縮機的耗能會降低SOFC發電系統的效率，故SOFC發電系統若操作於1.33 atm，可獲得最佳的發電效率。Virkar et al.曾以理論分析搭配美國 Westinghouse 公司的管狀 SOFC 電池堆性能測試，研究加壓效應對電池性能的影響[17]，他們發現，加壓效應可有效抑制陰極支撐以及陽極支撐的 SOFC 的濃度極化問題。而對電解質支撐 SOFC 而言，因其主要的極化問題為歐姆極化，故加壓效應對提升電池性能之助益相當有限。Henke et al.同樣以理論分析的方式研究加壓型 SOFC 的性能[18]，他們的結果顯示，加壓效應對於增加 OCV 值、降低活化極化以及擴展擴散極限都能有正面的幫助，但此助益在壓力值介於 1 ~ 5 atm 時較為顯著，5 ~ 20 atm 時，壓力效應對電池性能的影響則逐漸趨於不明顯。Recknagle et al.則是以 Star-CD 套裝軟體建立單流道電池堆三維數值模型[19]，即陽極端與陰極端都只考慮單一流道的單電池堆模型，模擬分析加壓型 SOFC 內的重組反應與電化

學反應，發現當操作壓力由 1 atm 增加至 10 atm 時，電池性能約增加 9%，而單電池堆內的最高溫度以及平均溫度約增加 3% (≈ 20 ^{o}C)。

實驗測試方面，美國 Honeywell 曾於 2001 年受美國能源部委託，建立實驗室規模的加壓式平板型 SOFC 單電池堆測試平台，並測試 1 ~ 2 atm 條件下的電池性能[20]。實驗結果顯示，當操作溫度為 800^{o}C，且操作電壓為 0.6 V 時，常壓條件下之單電池堆開始產生濃度極化，而加壓式 SOFC 則未有濃度極化現象產生。此外，兩者於操作電壓為 0.6 V 時的功率密度約相差 100 mW/cm^{2}。Zhou et al. [21]以管狀 SOFC 單電池堆進行實驗測試，並由熱力學與化學反應動力學討論壓力效應與溫度效應何者為主導電池性能之要素。結果顯示，增加操作溫度在熱力學上屬於負面的影響(降低 OCV)，但在化學反應動力學方面則為正面影響(增加反應率)；增加操作溫度則對兩方面都屬於正面影響，故壓力效應為主導電池性能變化的因素，且性能隨壓力增加而增加。Thomsen et al. [22]以阻抗頻譜量測的方式，研究壓力效應對鈕扣型 SOFC 氧離子傳輸機制的影響。他們發現，增加 SOFC 的操作壓力，可有助於改善陰極氧原子的吸附作用與離子的傳輸反應，而這對改善活化極化與歐姆極化都能有所幫助。日本 Eguchi 教授的團隊曾建立陽極半電池的高壓實驗平台，並進行 1 ~ 10 atm 的阻抗頻譜量測與分析，他們的數據顯示，陽極活

化過電位幾乎不受壓力效應的影響，但電池的操作壓力增加會使電化學反應更為激烈，進而增加濃度極化現象[23]。

最近，德國航太中心為了建立 SOFC 與氣渦輪機結合的複合式發電系統，也開始進行加壓型 SOFC 的實驗與數值模擬研究[24]。他們採用雙腔室的設計，即內腔室為高溫爐，外腔室為壓力容器。此外，由於該團隊的電池堆是採密封式設計，故需設計一對 Equalizing tanks 來平衡陽極與陰極端的壓力，避免壓力梯度過大而造成電池片破壞。他們的實驗結果顯示，當壓力由 1 atm 升至 2 atm 時，功率密度約增加 8.3%，但當壓力由 1 atm 升至 3 atm 時，則功率密度僅約增加 13.8%，顯示加壓效應在較低壓的環境效對電池性能影響較明顯。另外，韓國研究團隊 Lim et al. [25]則以德國能源研究中心(Forschungszentrum Juelich, FZJ)所開發的 F-design 平板型 SOFC 為基礎，建立加壓式 40-cell stack，並將其與微氣渦輪機結合。他們首先獨立測試加壓式 SOFC 電池堆於不同壓力條件下(1 atm ~ 3.5 atm)之性能，結果發現，當操作電壓固定於 30 V 時，壓力若由 1 atm 增加至 2 atm，則功率密度增加約 4.2%。而壓力由 2 atm 增加至 3.5 atm 時，功率密度的增加率則低於 1%。雖然他們已成功將 FZJ 所開發的平板型 SOFC 操作於高壓條件中，並成功與微氣渦輪機結合建立 5 kW 等級的複合發電系統。但作者於論文中特別強調，此

類型的電池堆在高壓環境下所造成的氣體洩漏問題仍未有效克服，且壓力爐與電池堆之間的壓力差不可大於 200 mbar，而多次實驗都因氣體洩漏或電池片破裂而失敗，且成功發電的複合發電系統在操作 1000 小時之後也會有明顯的劣化率。核研所目前所採用的電池堆設計就是和 FZJ 相似的雙進口單出口流場板，因此未來應也需克服高壓條件下的氣體洩漏問題。

參、研究方法與過程

本節將說明本計畫所採用之研究方法，包含創新加壓型固態氧化物燃料電池(SOFC)之實驗、密封材料洩漏率測試以及數值模擬分析。

一、創新加壓型固態氧化物燃料電池實驗

圖 1 為高壓測試平台的示意圖，此平台是以常壓型 SOFC 單電池堆性能測試平台為基礎[26,27]，沿用既有的氣體供應系統(圖 1 左上)、單電池堆設計(圖 1 左下)以及電池性能量測設備(圖 1 右下)，並新設計一套壓力監控系統(圖 1 右上) 和雙腔室高壓容器(圖 1 中)。雙腔室高壓容器之內腔室為高溫爐，外腔室為 10 大氣壓等級的高壓爐。我們特將導引反應物進入單電池堆的氣體管線彎折成蛇形，以充份預熱反應氣體，避免電池片因熱震(thermal shock)而破裂。

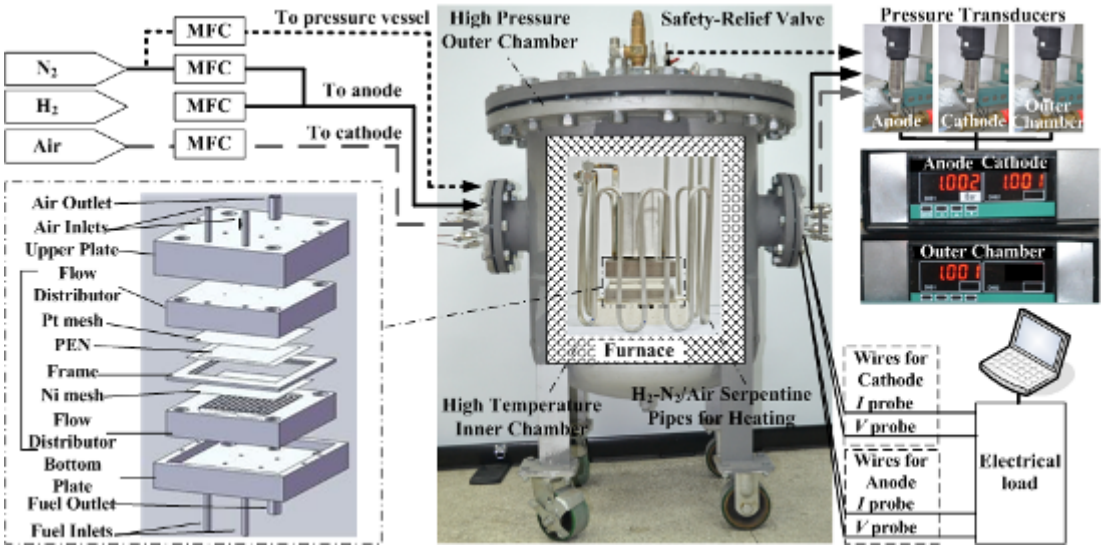

圖 1. 加壓型 SOFC 性能測試平台示意圖。

本計畫採用 seal-less 的方式組裝單電池堆，電池片是向 H.C. Starck 公司購買的陽極支撐 ASC III 電池片，有效反應面積則為 40 mm × 40 mm。集電層方面，陰極為白金網，陽極為白金網加鎳網，其中鎳網置於電池片與白金網之間。兩端電極之集電層分別焊接八條導線，同一端電極取四條作為電壓導線，另四條則作為電流導線。焊接於集電層上的導線都是白金線，這是因為在測試過程中發現，鎳線在加壓實驗中容易被氧化，且白金線的熔點(1973 K)略高於鎳線(1808 K)，較不易因高溫爐內所產生的燃燒現象而遭熔斷。為了避免鉻毒化的問題影響實驗結果，本研究使用氧化鋁陶瓷材料製作流場板。圖 2 為本研究所採用的兩組不同之流場板設計，兩者的尺寸完全相同，唯一的差異為 Design I 未加裝導流板，Design II 則於進口區加裝導流板。

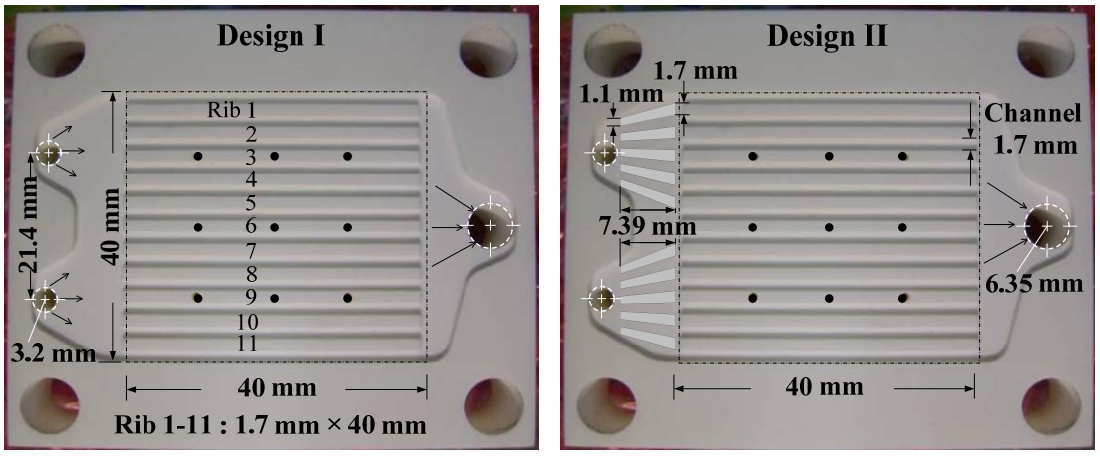

圖 2. 兩組不同設計之氧化鋁陶瓷流道板。

為能獲得具可靠度且具重複性之實驗數據，本計畫建立一套加壓 SOFC 單電池堆性能測試之標準實驗流程，其中最主要的步驟，乃為單電池堆的升降壓程序。進行高壓實驗前，需以 0.02 atm/min 的升壓速率緩慢將壓力提升至實驗所設定的數值，且升壓過程須保持陽極與陰極，以及單電池堆與壓力容器的壓力差低於 50 mbar，以避免電池片因壓力梯度過大而破裂。此外，由我們過去的經驗得知，陽極、陰極以及壓力容器的操作壓力不易調整至完全相同，故我們在壓力差低於 50 mbar 的前提下，維持陽極壓力最高，陰極次之，壓力容器最低。

極化曲線量測方面，採用定電流模式，量測電壓與輸出功率隨電流的變化率，控制電流間距為 0.2 A，單點測量時間為 30 秒。當電池操作於低電壓或高電流條件時，濃度損失會明顯增加，觸媒因反應過於激烈容易造成電池損壞，因此一般電池運作不會操作在此

低電壓或高電流條件，故本實驗負載最低電壓值為 0.7 V，而相對應之最高電流密度值不可高於 300 mA/cm^2。阻抗頻譜量測方面，採雙極量測，並以定電壓模式進行，控制電壓分別為 OCV 及 0.7 V，頻率測量範圍皆為 50 mHz ~ 3 kHz，電壓振幅為 50 mV。

二、密封材料洩漏率實驗

圖 3 為已建立的實驗平台示意圖，重要組件含以不鏽鋼 SS316 製作的測試元件(元件下半部份裝置於高溫爐內部)、高溫爐外部的氣體容器、質流量計、壓力計以及洩壓閥。依測試對象的不同，我們必須施與測試元件不同的壓應力，因此在測試元件的上板對稱地裝上四根可替換的彈簧，由彈簧的彈性係數與變形量，即可估算出所提供的壓應力。

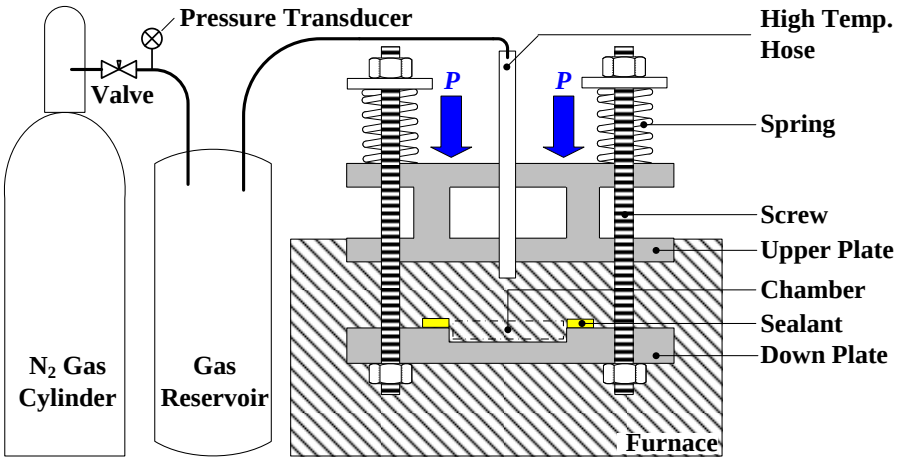

圖 3. 高溫氣體洩漏率測試平台示意圖。

為了避免高溫操作條件對彈簧的彈性係數造成影響，彈簧將裝置在

高溫爐外部，且在必要時加裝冷卻系統。如此一來，我們將能在實驗測試的過程中保持固定的壓應力。測試元件的下板將銑刻出一氣體腔室，實驗進行時，此氣體腔室的壓力與高溫爐外部的氣體容器(gas reservoir)相同，故將壓力計量測到的數據代入 Le et al. [9]所提出的計算公式，即可求得不同密封材料的氣體洩漏率。公式如下：

$$L = (P_i - P_f)V / (P_f \Delta t\, C) \quad (1)$$

其中 L 為氣體洩漏率(sccm/cm)、V 為外部氣體容器的體積(cm^3)、P 為氣體壓力(Kgf/cm^2)、t 為時間(min)、C 為密封材料之周長(cm)、下標 i 與 f 則表示初始值與最終值。

三、化學反應流數值模擬

本計畫利用數值模擬方法，分別針對加壓型 SOFC 單電池堆以及不同尺寸之棋盤狀流道單電池堆進行模擬分析。數值模擬所採用的各項統御方程式及參數說明，請參閱本團隊已發表於 J. Power Sources 之論文[29]。圖 4 為本研究所建立的兩組三維加壓型 SOFC 單電池堆數值模型，配合所進行的實驗，數值模擬同樣採用 co-flow 的流場配置方式，即陰極與陽極的流向相同。

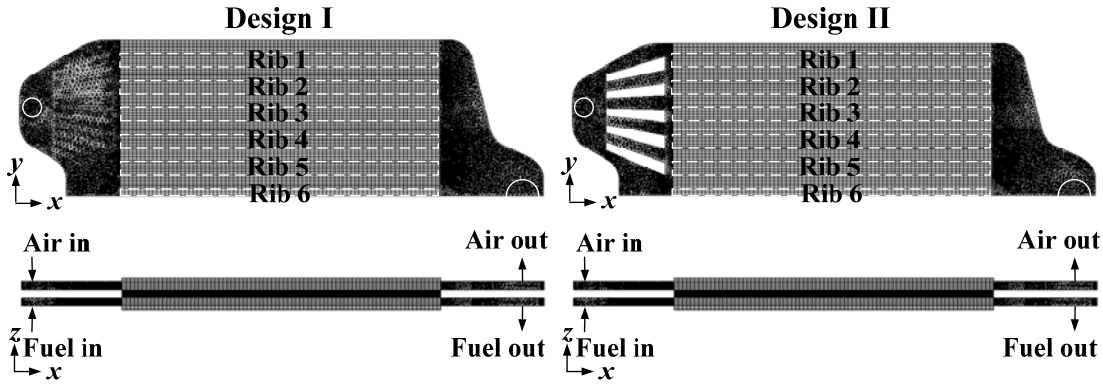

圖 4. 配合圖 2 之設計所建立的兩組三維數值模型。

本研究的化學反應流數值模型中含括多種次模組，例如用 ideal gas law 計算各種反應物與生成物之密度，以 kinetic theory 計算流體的黏滯係數與熱傳導係數等。因此，即使操作壓力改變，反應物與生成物的物理化學性質仍可被合理的估算，並導入運算的統御方程式中，唯獨電化學反應次模組中的重要參數，交換電流密度(exchange current density)，需視操作壓力的改變而做合理的調整。

肆、主要發現與結論

本節彙整本計畫所獲得的研究成果，最後做總結並規劃未來擬持續進行之研究工作。

一、結果與討論

以下說明本計畫所獲得之研究成果及主要發現，包含(1)加壓型 SOFC 性能量測與模擬分析；(2)壓縮式密封材料洩漏率測試；與(3)棋盤狀流道尺寸效應對單電池堆性能之影響。

(一) 加壓型 SOFC 性能量測與模擬分析

考慮以氫氣與氧氣為反應物的 SOFC 系統，並將其操作於 850°C，則加壓效應對 SOFC 輸出電壓的影響可利用 Nernst Equation 進行估算，如下式所示：

$$\Delta V = 0.024 \ln\left(\frac{P_2}{P_1}\right) \tag{2}$$

圖 5 分別為 Design II (圓形實心符號)、Design I (圓形空心符號)的實驗量測 OCV 值，以及利用(2)式所計算出來的 OCV 數據。

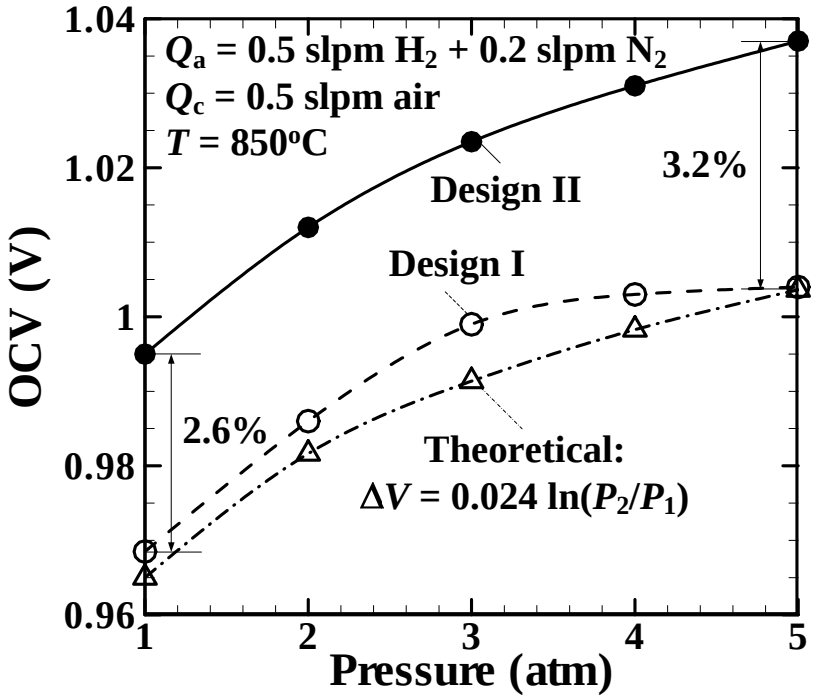

圖 5. 壓力效應對 OCV 的影響。

結果顯示，使用兩種不同流場板所量測到的 OCV 值皆會隨操作壓力

增加而增加，且都和 Nernst Equation 所預測的趨勢相似，即當壓力由 1 atm 增加至 5 atm 時，OCV 可被提升約 4%。此外，我們發現改善流場板內的流場均勻度，可有助於陽極觸媒的均衡使用，並進一步提升 SOFC 的 OCV 值。

我們進一步分析加壓效應對於 SOFC 阻抗(area specific resistance, ASR)的影響，ASR 值可由下式定義：

$$\mathrm{ASR} = \frac{\mathrm{E_{mf}} - V}{i} \tag{3}$$

其中 $\mathrm{E_{mf}}$ 為電池的電動勢(electromotive force)，即兩電極間的電位差，V 為電池操作電壓，i 則為電壓 V 時之電流值。ASR 所代表的物理意義為燃料電池的歐姆阻抗(ohmic resistance, R_Ω)以及電極極化阻抗(electrode polarization resistance, R_p)之總和，故可將 ASR 區分為五大項：

$$\mathrm{ASR} = R_{\Omega,\mathrm{e}} + R_{\Omega,\mathrm{connect}} + R_{\mathrm{p,elechem}} + R_{\mathrm{p,diff}} + R_{\mathrm{p,conver}} \tag{4}$$

(4)式中，$R_{\Omega,\mathrm{e}}$ 為電池片之歐姆阻抗，與電極材料和厚度有關；$R_{\Omega,\mathrm{connect}}$ 為接觸阻抗；$R_{\mathrm{p,elechem}}$ 為電池三相邊界(triple-phase boundary)上之化學或電化學反應所產生的阻抗；$R_{\mathrm{p,diff}}$ 為氣體擴散的阻抗；$R_{\mathrm{p,conver}}$ 則為氣體轉換的阻抗(如氫氣與氧氣的氧化還原反應)。正因為 ASR 值幾乎已包含所有的電池性能極化機制，如何將各種阻抗由 ASR 中抽

離並進行分析與研究，是許多研究團隊努力的目標。

目前 SOFC 之 ASR 量測方面的研究可大致分為兩大部分，一部分的學者將 ASR 視為代表 SOFC 歐姆阻抗的指標參數，舉例來說，美國能源部所出版的 *Fuel Cell Handbook* 中提及，ASR 的計算應採用操作電壓介於 0.85 V ~ 0.6 V 的區間，因為此區間的電流-電壓曲線幾乎呈線性關係，且可被直接視為電池的歐姆阻抗值[29]。此外，歐盟 Real-SOFC 計畫所制定的單電池測試規範，亦明確定義 ASR 的計算方法，應採用 0.75 V ~ 0.85 V 之間的電流-電壓曲線斜率[30]，而德國能源研究中心也採用同樣的 ASR 計算方式[31]。然而，有另一部分的學者卻認為上述的 ASR 計算方式僅適用於電解質支撐 SOFC，因為電解質支撐 SOFC 主要的阻抗來自電解質材料的歐姆值，電極支撐 SOFC 會有較明顯的活化極化以及濃度極化問題，不易定義出代表歐姆極化的線性區域，故不適合使用該計算方式[32,33]。Gemmen et al. [33]認為，ASR 不只是電流的函數，同時也應為時間的函數。

根據 JRC 之規範[30]，電池性能之優劣可利用三個參數來進行比較，分別為 OCV、操作於 0.7 V 之功率密度以及面積比電阻(ASR)，其中 ASR 被定義為在 0.75 V ~ 0.85 V 區間的極化曲線斜率[30]。

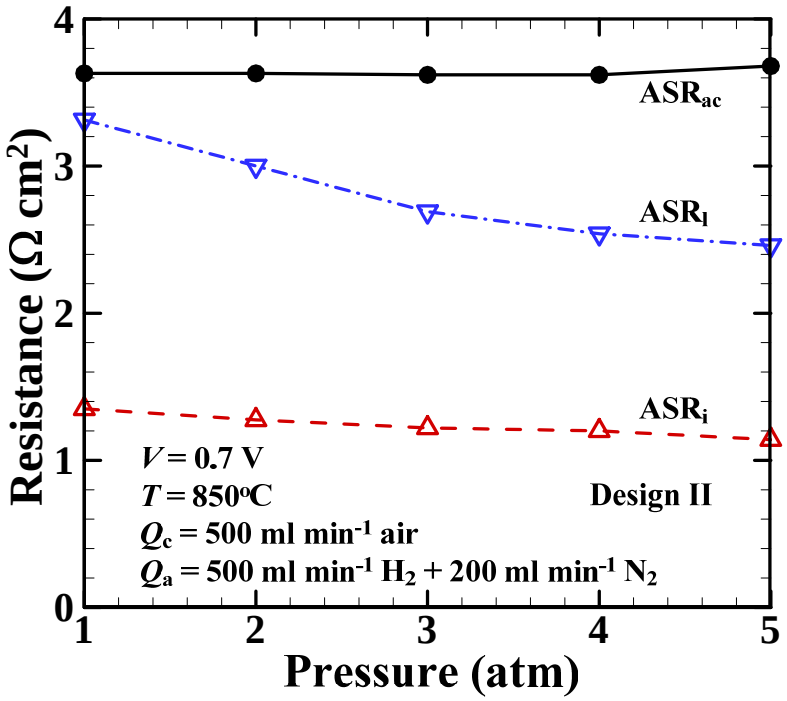

圖 6. 壓力效應對 ASR 的影響。

圖 6 為本次實驗所獲得的不同計算方式的 ASR 值隨壓力變化關係圖，ASR_{ac} 表示由頻譜阻抗儀所量測的值；ASR_l 是由電壓-電流曲線圖採用德國能源研究中心的計算方式[31]所得值；ASR_i 是採用積分的方式所求出的值。可發現在常壓條件下，單電池堆的 ASR_l 值約為 3.31 Ω cm^2，而在 5 atm 條件下，ASR_l 值為 2.46 Ω cm^2，故當 P = 1 ~ 5 atm 時，加壓效應有助於降低單電池堆的 ASR 值達 26%。而 ASR_{ac} 與 ASR_i 卻不會隨著壓力的改變而增加，原因是採用德國能源研究中心的計算方式[31]所得值，其中包含活化極化以及濃度極化的現象。而 ASR_{ac} 與 ASR_i 所得的值只含歐姆阻抗。

ASR_I 為表示電池歐姆阻抗的重要參數之一，可被視為單電池堆內多種阻抗的總和，其中包含各元件的電阻值、各元件間的接觸阻抗、以及電子與離子傳輸的內部阻抗等。由於材料之電阻值以及接觸阻抗不會因加壓而改變，故加壓效應應是改善電子與離子傳輸的內部阻抗，進而降低 ASR_I 值。由於加壓有助於使更多的反應物進入多孔電極內部進行反應，因此增加了反應物碰撞觸媒的機率，即增加三相邊界(triple-phase boundary, TPB)的長度，此將有助於縮短離子或電子傳輸的路徑，降低阻抗值。

同樣依據 JRC 的規範，我們將單電池堆操作於 0.7 V 的電池性能進行分析與比較。為同時了解加壓效應對燃料與空氣的使用率之影響，我們也利用下列公式計算氫氣與氧氣的使用率：

$$\mathrm{H_2\ usage\,(moles\,s^{-1})} = \frac{In}{2F} = 5.18\times10^{-6}\ I \tag{5}$$

其中 I 為電流(A)、n 為電池數。

圖 7 顯示加壓效應對於電池性能有明顯的助益，當 P 由 1 atm 增加至 5 atm 時，功率密度約增加約 27%，而由圖 7 燃料使用率的增加則可以發現，增加單電池堆的操作壓力，有助於提升反應物擴散至多孔電極表面的機制，讓更多的反應物參與反應，進而提升電池性能。綜合本次實驗所進行的單電池堆極化曲線量測與分析之結

果，我們發現加壓效應對於抑制單電池堆的三種主要極化機制都能有所助益，且影響單電池堆之濃度極化最大(0.7 V 時之功率密度提昇約 25%)，歐姆極化次之(ASR_I 值降低約 18%)，活化極化最小(OCV 增加約 3%)。

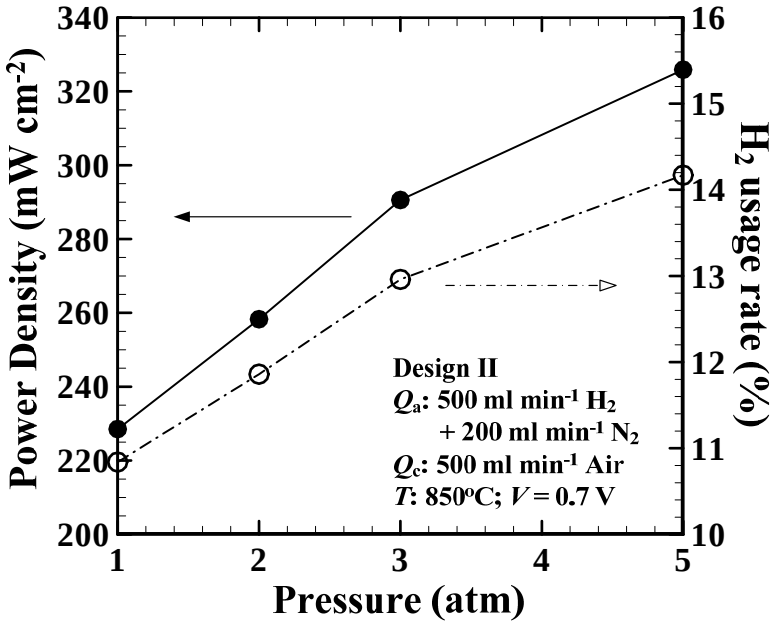

圖 7. 加壓效應對燃料使用率之影響

圖 8 為兩組採用不同流場板設計單電池堆於不同加壓條件下之極化曲線，其中符號與數線分別為實驗量測與數值模擬之數據。如圖所示，當電流密度固定於 300 mA cm^{-2}，操作壓力由 1 大氣壓增加至 5 大氣壓時，Design I 與 Design II 的功率密度約增加 13%與 16%。

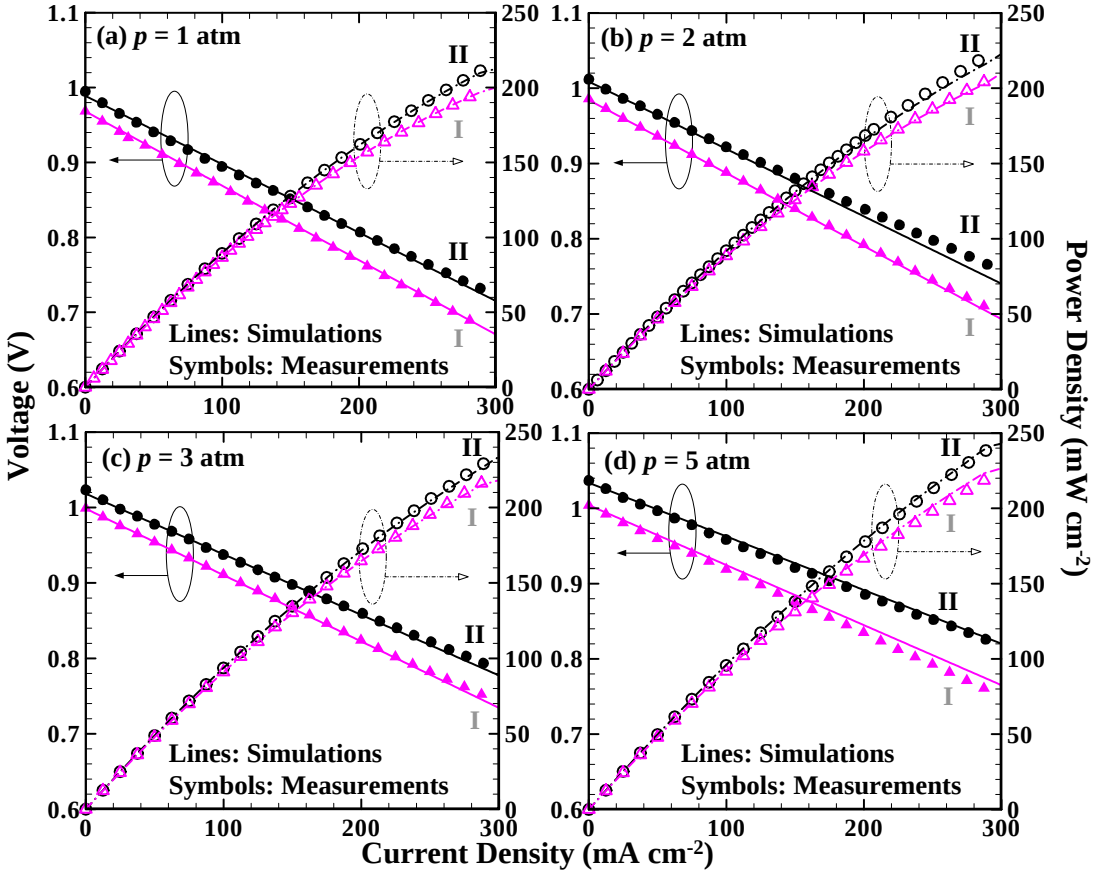

圖 8. 兩組採用不同流場板設計單電池堆分別於(a) 1 atm, (b) 2 atm, (c) 3 atm 以及(d) 5 atm 條件下之性能。

此外，比較圖 8 (a-d)可以發現，在常壓條件下，採用 Design II 流場板，即加裝導流板設計之流場板，其電池性能比未加導流板設計(Design I)高約 13%。當壓力增加至 5 大氣壓，電池性能的差異約為 16%，顯示流場均勻度效應與加壓效應同樣能對提升電池性能有所貢獻。

(二) 壓縮式密封材料洩漏率測試

我們首先針對 Le et al. [9]所提出的新型密封材料(融煉石英與陶

瓷纖維之複合材料)製作程序進行測試，並提出各製程參數的優化值，其標準程序為：(1)烘烤陶瓷纖維，以 700 °C 持續烘烤 1 小時，去除纖維紙內部的有機雜質；(2)將烘烤過之陶瓷纖維浸泡於二氧化矽水溶液中，並以恆溫震盪器持續搖晃器皿，使二氧化矽水溶液充份滲入纖維紙內部；(3)於高溫下(超過 100°C)烘烤 5 小時，將水蒸氣去除後，可使二氧化矽結晶附著於陶瓷纖維孔隙；(4)將陶瓷纖維施予預壓力，可使二氧化矽結晶能更緊密地填滿纖維孔隙。測試結果顯示，烘烤溫度(T_{dry})與預壓壓力(p_c)為影響新型密封材料洩漏率的兩個主要參數，其優化值分別為 T_{dry} = 160°C，p_c = 10 MPa。

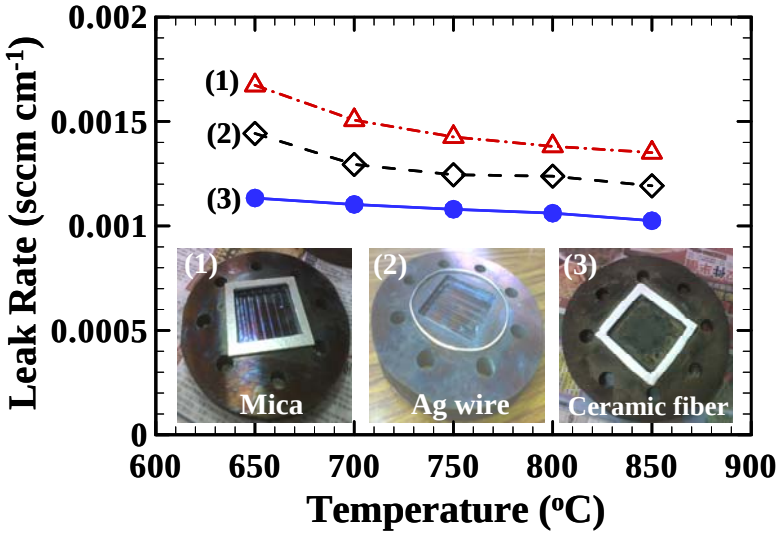

圖 9. 不同壓縮式密封材料於高溫條件下之洩漏率。

我們利用優化的製程製做新型密封材料，並量測其與銀線以及雲母，在不同溫度(T = 650 °C ~ 850 °C)條件下之洩漏率(R_l 值)，如圖

9 所示，增加操作溫度會使銀線與雲母的厚度增加，進而降低 R_l 值。然而，此膨脹現象卻可能導致 SOFC 的電池片被破壞。另一方面，新型密封材料的 R_l 值幾乎不會隨溫度而改變，顯示其具備高物理穩定度。當操作溫度為 850 ^oC 時，新型密封材料的 R_l 值僅為 7.62×10^{-4} sccm/cm，優於銀線和雲母材料。

二、結論與建議

綜合本研究所獲得的各項數據，包含實驗量測與數值模擬，我們歸納出下列幾點結論、具體成果與建議：

(1) 本團隊已建立國內首套加壓型單電池堆實驗測試平台，並已進行多組實驗測試，所累積之實作經驗與研究能量，將有助於核研所建置 SOFC 與 GT 結合之複合發電系統。未來將進一步利用阻抗頻譜分析技術，深入研究加壓效應對於 SOFC 極化機制之影響。

(2) 藉由高溫氣密測試實驗，我們提出以氣相式二氧化矽和陶瓷纖維製作密封材料的優化製備程序及相關參數，並發現在高溫條件下，該新型密封材料之氣密性優於傳統的雲母與銀線。由於此新型密封材料成本低且製備容易，應具備實用價值。未來我們將進行高壓高溫條件下之氣密測試，以評估該密封材料應用於加壓型 SOFC 之適用性。

(3) 已與李堅雄博士共同發表一篇 SCI 論文於 Journal of Power Sources，內容請參見附件。

(4) 發表兩篇會議論文至 2011 European Fuel Cell Conference & Exhibition 會議。題目分別為：(1) Planar solid oxide fuel cells: cell performance and impedance measurements of single-cell stacks using pin-type flow channels with various sizes；(2) A high-pressure double-chamber SOFC platform for cell performance measurements using different flow distributors。此會議已於今年 12 月 14 日 ~ 16 日在義大利羅馬舉行。本團隊由黃家明博士代表參加，並口頭

報告上述兩篇論文。

(5) 投稿一篇會議論文至第 6 屆全國氫能與燃料電池研討會，題目為“Implementation and Testing of New Compressive Sealant for Planar SOFC”，此會議已於今年 10 月 28～29 日在宜蘭大學舉辦，已由計畫主持人碩一學生謝易達先生前往報告。

(6) 投稿一篇會議論文至中華民國力學學會年會暨第 35 屆全國力學研討會，題目為“固態氧化物燃料電池-陽極半電池碳沉積阻抗頻譜量測”，此會議於今年 11 月 18 ~ 19 日在國立成功大學舉辦。將由計畫主持人碩一學生吳佩真小姐前往報告。

伍、參考文獻

[1] Park, S. and Kim, T.S., Comparison between pressurized design and ambient pressure design of hybrid solid oxide fuel cell-gas turbine systems, *J. Power Sources*, Vol. **163**, pp. 490-499, 2006.

[2] Lee, C.H., Lee, M.C., Hwang, C.S., Lee, R.Y. and Lin, L.F., SOFC development at INER, *Int. J. Appl. Ceram. Technol.*, Vol. **4**, pp. 339-349, 2007.

[3] Liu, H.C., Lee, C.H., Shiu, Y.H., Lee, R.Y. and Yan, W.M., Performance simulation for an anode-supported SOFC using Star-CD code, *J. Power Sources*, Vol. **167**, pp. 406-412, 2007.

[4] Chiang, L.K., Liu, H.C., Shiu, Y.H., Lee, C.H. and Lee, R.Y., Thermal stress and thermo-electrochemical analysis of a planar anode-supported solid oxide fuel cell: Effects of anode porosity, *J. Power Sources*, Vol. **195**, pp. 1895-1904, 2010.

[5] Yen, T.H., Hong, W.T., Huang, W.P., Tsai, T.C., Wang, H.Y., Huang, C.N. and Lee, C.H., Experimental investigation of 1 kW solid oxide fuel cell system with a natural gas reformer and an exhaust gas burner, *J. Power Sources*, Vol. **195**, pp. 1454-1462, 2010.

[6] Veyo, S.E., Shockling, L.A., Dederer, J.T., Gillett, J.E. and Lundberg, W.L., Tubular solid oxide fuel cell/gas turbine hybrid cycle power systems: status, *J. Eng. Gas. Turbines Power-Trans. ASME*, Vol. **124**, pp.845-849, 2002.

[7] Yang, W.J., Park, S.K., Kim, T.S., Kim, J.H., Sohn, J.L. and Ro, S.T., Design performance analysis of pressurized solid oxide fuel cell/gas turbine hybrid systems considering temperature constraints, *J. Power Sources*, Vol. **160**, pp. 462-472, 2006.

[8] Fergus, J.W., Sealants for solid oxide fuel cells, *J. Power Sources*, Vol. **147**, pp. 46-57, 2005.

[9] Le S., Sun, K., Zhang, N., An, M., Zhou, D., Zhang, J. and Li, D., Novel compressive seals for solid oxide fuel cells, *J. Power Sources*, Vol. **161**, pp. 901-906, 2006.

[10] Singhal, S.C. and Kendall, K., *High temperature solid oxide fuel cells: fundamentals, design and applications*, Elsevier Ltd.,

Kidlington, UK, 2003.

[11] Larminie, J. and Dicks, A., *Fuel cell systems explained*, 2nd Eds., John Wiley & Sons Ltd., West Sussex, England, 2003.

[12] Yi, Y., Rao, A.D., Brouwer, J. and Samuelsen, G.S., Analysis and optimization of a solid oxide fuel cell and intercooled gas turbine (SOFC-ICGT) hybrid cycle, *J. Power Sources*, Vol. **132**, pp. 77-85, 2004.

[13] Arsalis, A., Thermoeconomic modeling and parametric study of hybrid SOFC–gas turbine–steam turbine power plants ranging from 1.5 to 10 MWe, *J. Power Sources*, Vol. **181**, pp. 313-326, 2008.

[14] Ni, M., Leung, M.K.H. and Leung, D.Y.C., Parametric study of solid oxide fuel cell performance, *Energy Conv. Manag*., Vol. **48**, pp. 1525–1535, 2007.

[15] Patcharavorachot, Y., Arpornwichanop, A. and Chuachuensuk, A., Electrochemical study of a planar solid oxide fuel cell: role of support structures, *J. Power Sources*, Vol. **177**, pp. 254-261, 2008.

[16] Bo, C., Yuan, C., Zhao, X., Wu, C.B. and Li, M.Q., Parametric analysis of solid oxide fuel cell, *Clean Techn. Environ. Policy*, Vol. **11**, pp. 391-399, 2009.

[17] Virkar, A.V., Fung, K.Z. and Singhal, S.C., The effect of pressure on solid oxide fuel cell performance, *Proceedings of the Third International Symposium on Ionic and Mixed Conducting Ceramics*, 1997.

[18] Henke, M., Kallo, J., Friedrich, K.A. and Bessler, W.G., Influence of pressurization on SOFC performance and durability: a theoretical study, *Fuel Cells*, Vol. **11**, pp. 581-591, 2011.

[19] Recknagle, K.P., Ryan, E.M., Koeppel, B.J., Mahoney, L.A. and Khaleel, M.A., Modeling of electrochemistry and steam-methane reforming performance for simulating pressurized solid oxide fuel cell stacks, *J. Power Sources*, Vol. **195**, pp. 6637-6644, 2010.

[20] Honeywell, *Solid oxide fuel cell hybrid system for distributed power generation*, Quarterly Technical Progress Report, DE-FC26-01NT40779, 2002.

[21] Zhou, L., Chen, M., Yi, B., Dong, Y., Cong, Y. and Yang, W.,

Performance of an anode-supported tubular solid oxide fuel cell (SOFC) under pressurized conditions, *Electrochim. Acta*, Vol. **53**, pp. 5195-5198, 2008.

[22] Thomsen, E.C., Coffey, G.W., Pederson, L.R. and Marina, O.A., Performance of lanthanum strontium manganite electrodes at high pressure, *J. Power Sources*, Vol. **191**, pp. 217–224, 2009.

[23] Kikuchi, R., Yano, T., Takeguchi, T. and Eguchi, K., Characteristics of anodic polarization of solid oxide fuel cells under pressurized conditions, *Solid State Ionics*, Vol. **174**, pp. 111-117, 2004.

[24] Seidler, S., Henke, M., Kallo, J., Bessler, W.G., Maier, U. and Friedrich, K.A., Pressurized solid oxide fuel cells: experimental studies and modeling, *J. Power Sources*, Vol. **196**, pp. 7195-7202, 2010.

[25] Lim, T.H., Song, R.H., Shin, D.R., Yang, J.I., Jung, H., Vinke, I.C. and Yang, S.S., Operating characteristics of a 5 kW class anode-supported planar SOFC stack for a fuel cell/gas turbine hybrid system, *Int. J. Hydro. Energy*, Vol. **33**, pp. 1076-1083, 2008.

[26] Huang, C.M., Shy, S.S., Li, H.H. and Lee, C.H., The impact of flow distributors on the performance of planar solid oxide fuel cell, *J. Power Sources*, Vol. **195**, pp. 6280-6286, 2010.

[27] Shy, S.S., Huang, C.M., Li, H.H. and Lee, C.H., The impact of flow distributions on the performance of solid oxide fuel cell – Part II: Electrochemical impedance measurements, *J. Power Sources*, Vol. **196**, pp. 7555-756, 2011.

[28] Huang, C.M., Shy, S.S. and Lee, C.H., On flow uniformity in various interconnects and its influence to cell performance of planar SOFC, *J. Power Sources*, Vol. **183**, pp. 205-213, 2008.

[29] EG & G Services, *Fuel Cell Handbook*, U.S. Department of Energy, Office of Fossil Energy, National Energy Technology Laboratory, Morgantown, W.V., 2004.

[30] Marco, G.D., Pilenga, A., Honselaar, M., Malkow, T., Tsotridis, G., Janssen, A., Rietveld, B., Vinke, I. and Kiviaho, J., SOFC single cell performance and endurance test modules, *JRC Scientific and Technical Report*, TM SOFC 01-04 LD/05-08 HD, Joint Research Centre Scientific and Technical Reports, 2010.

[31] Steinberger-Wilckens, R., Blum, L. and Buchkremer, H., Overview of the development of solid oxide fuel cells at Forschungszentrum Juelich, *Int. J. Appl. Ceram. Tech.*, Vol. **3**, pp. 470-476, 2006.

[32] Kim, J., Virkar, A. and Fung, K., Polarization effects in intermediate temperature, anode-supported solid oxide fuel cells, *J. Electrochem. Soc.*, Vol. **146**, pp. 69-78, 1999.

[33] Gemmen, R.S., Williams, M.C. and Gerdes, K., Degradation measurement and analysis for cells and stacks, *J. Power Sources*, Vol. **184**, pp. 251-259, 2008.

附件一、本年度發表於 Journal of Power Sources 的論文(SCI)

Journal of Power Sources 196 (2011) 7555–7563

Contents lists available at ScienceDirect

Journal of Power Sources

journal homepage: www.elsevier.com/locate/jpowsour

The impact of flow distributors on the performance of solid oxide fuel cell—Part II: Electrochemical impedance measurements

S.S. Shy[a,b,*], C.M. Huang[a], H.H. Li[a], C.H. Lee[c]

[a] Department of Mechanical Engineering, National Central University, Jhong-li 32001, Taiwan
[b] Center for Energy Research, College of Engineering, National Central University, Taiwan
[c] Institute of Nuclear Energy Research, Lung-tan, Tao-yuan 32546, Taiwan

ARTICLE INFO

Article history:
Received 15 February 2011
Received in revised form 7 April 2011
Accepted 8 April 2011
Available online 22 April 2011

Keywords:
Planar anode-supported solid oxide fuel cell
Flow distributors
Electrochemical impedance spectroscopy
Anodic re-oxidation
Anodic microstructures

ABSTRACT

This paper presents newly measured electrochemical impedance spectra of two sets of nearly identical single-cell stacks except using different designs of flow distributors for planar solid oxide fuel cells (SOFCs). It is found that by using small guide vanes around the feed header of commonly used rib-channel flow distributors to improve significantly the degree of flow uniformity, values of ohmic and polarization resistances of the single-cell stack can be decreased by 32% and 60% as compared to that without using guide vanes under the same experimental conditions at 0.6 V and 850 °C. This finding explains why by improving flow uniformity in interconnects can result in more than 10% increase of the cell power density. Moreover, the higher resistances measured for the case without using guide vanes are attributed to the anodic re-oxidation behavior due to non-uniform flow distributions in interconnects, as also verified by SEM images of anodic microstructures. These results show that the improvement of flow uniformity in flow distributors is useful to increase the performance and the longevity of planar SOFCs.

1. Introduction

This is the third paper emanating from a series of numerical and experimental studies [1,2] aiming to address the impact of flow distributors on the cell performance of planar solid oxide fuel cell (SOFC). In it we report for the first time the newly measured electrochemical impedance spectra and anodic re-oxidation microstructures of two sets of nearly identical single-cell stacks having flow distributors in both anode and cathode under the same operating conditions except that different designs of flow distributors are applied in these two single-cell stacks. Hence, the obtained results can be used to explain why by improving flow uniformity in interconnects not only can result in more than 10% increase of the cell power density but also can avoid the cell degradation caused by the anodic re-oxidation.

In our previous numerical and experimental studies [1,2], we used the term "single-cell stack", same as other research groups such as Yakabe et al. [3,4], to distinguish from "single cell" that only consisted of a positive electrode–electrolyte–negative electrode (PEN) and current collectors without flow distributors. The first paper dealt with the issue of "*what*", in which four different designs of commonly used rib-channel flow distributors having different degrees of flow uniformity were proposed [1]. It should be noted that the flow uniformity has been verified by measuring flow velocities and thus flow rates in each of twelve rib-channels, as can be found from Figs. 6 and 7 of Ref. [1]. These four different flow distributors were then used in several 3D electrochemical numerical models to predict the influence of flow uniformity in interconnects on the cell performance of planar SOFC [1]. It was found that a new design, using simple small guide vanes equally spaced around the feed header of the double-inlet/single-outlet rib-channel flow distributor, can significantly improve the degree of flow uniformity in interconnects, resulting in an increase of the peak power density (PPD) of single-cell stacks up to 11% [1]. In order to validate the numerical finding [1] and show "*how*" exactly the cell performance of single-cell stacks would vary with a change in the degree of flow uniformity, a real SOFC test rig was established, as presented in our second paper [2]. In [2], the power generating characteristics of two sets of nearly identical Ni–YSZ anode-supported single-cell stacks under exactly the same experimental conditions, except using or not using small guide vanes around the feed header of rib-channel flow distributors, were measured and compared. Hence, the numerical result indicating that by improving flow uniformity in interconnects can result in more than 10% increase of the cell power density was then experimentally validated. Using the same methodology as in [2] and further applying the electrochemical impedance spectroscopy (EIS) as well as the SEM microstructure visualization, the present study measures the

* Corresponding author at: Department of Mechanical Engineering, National Central University, 300 Jhong-da Road, Jhong-li, Tao-yuan 32001, Taiwan.
Tel.: +886 3 426 7327; fax: +886 3 427 6157.
E-mail address: sshy@ncu.edu.tw (S.S. Shy).

0378-7753/$ – see front matter © 2011 Elsevier B.V. All rights reserved.
doi:10.1016/j.jpowsour.2011.04.021

impedance spectra and the anodic re-oxidation microstructures for the aforementioned two sets of nearly identical single-cell stacks using different flow distributors. Thus, the final "*why*" issue concerning the impact of flow distributors on the performance and the anodic degradation of planar SOFC can be addressed.

The EIS technology, also known as the AC impedance technology, is a very useful tool for the investigation of the corrosions of materials, the performance of electrochemical devices, and the degradation mechanisms in SOFCs, see for instances Refs. [5–14] among many others. Because almost all kinds of transport phenomena in any given electrochemical devices including those in SOFCs have their own inherent electrochemical rates, the complex diffusion processes and electrochemical degradation mechanisms in SOFCs can be thus diagnosed by the EIS technology. For a typical impedance measurement of any electrochemical devices, a small perturbed voltage signal, $V(t) = V_0 \cos(\omega t + \varphi)$, is commonly applied onto the device to obtain a current response, $I(t) = I_0 \cos(\omega t + \psi)$, where V_0 and I_0 are the amplitudes of the voltage signal and the current response, ω is the angular frequency ($\omega = 2\pi f$), and φ and ψ are the initial phase angles of the voltage signal and the current response. Similar to the Ohm's law, the expression of the voltage signal and the current response can be converted from a time domain to a complex frequency domain via the Fourier transformation. Thus, the impedance function $Z(i\omega) = V(i\omega)/I(i\omega)$, where the imaginary number i; $(-1)^{0.5}$; $\exp(i\pi/2)$ indicating an anticlockwise rotation of the impedance vector by $\pi/2$ relative to the x-axis. In the complex plane, the real part of the impedance function is denoted as $\mathrm{Re}(Z)$; $Z' = |Z|\cos(\theta)$ and the imaginary part $\mathrm{Im}(Z) \equiv Z'' = |Z|\sin(\theta)$, where the phase difference $\theta = \varphi - \psi = \tan^{-1}(Z''/Z')$ and $|Z| = [(Z')^2 + (Z'')^2]^{1/2}$. Therefore, the plot of $-\mathrm{Im}(Z)$ against $\mathrm{Re}(Z)$ is the well-known Nyquist plot providing the information on the ohmic and polarization resistances, R_Ω and R_P, of the measured electrochemical device for electrochemical performance analyses [5–11]. However, the important frequencies associated with specific data points on these impedance spectra curves cannot be directly found from the Nyquist plot, but they can be obtained from the Bode plot indicating the impedance and the phase-shift as a function of the frequency [11]. In this study, both the Nyquist and the Bode plots for the aforementioned two sets of single-cell stacks using different flow distributors are measured and compared in order to explain the final "*why*" issue concerning the impact of flow distributors on the cell performance and the anodic degradation of planar SOFC. For a detail treatment on key concepts of EIS models and measurements, the reader is directed to Refs. [11,12].

Concerning the anodic degradation of planar SOFC, Gong et al. [13] categorized the sulfur-tolerant anode materials for the application of SOFC and highlighted possible combined designs of available materials in order to achieve a balance between stability and performance of the anode materials. Also, Iwanschitz et al. [14] investigated the anodic degradation of SOFC upon reduction and oxidation (redox) cycling, one of the major degradation mechanisms in SOFC, and they reported a decrease of the length of the triple-phase boundary due to the changes of the anodic microstructures during the operation of SOFC that can block the mass diffusion pathway of supplied gases. Furthermore, Liu et al. [15] investigated the re-oxidation and reduction of a NiO–YSZ/YSZ/LSM–YSZ anode-supported button cell by monitoring variations of the ohmic resistance under the open-circuit voltage (OCV) condition. They found that values of R_Ω increase with the anodic re-oxidation, because the Ni re-oxidation to NiO can increase the resistance of the electron transfer in anode. Similarly, Laurencin et al. [16] investigated damage mechanisms of the Ni–YSZ cermet re-oxidation in an anode-supported cell using a direct air oxidation (i.e., fuel shutdown) or using an ionic current (i.e., fuel starvation). In the latter case using fuel starvation, a thin layer of the cermet was electrochemically re-oxidized at 800 °C and then reduced under a hydrogen stream, by which such a redox cycle was repeated until the occurrence of serious cell degradation [16]. These EIS data obtained under the OCV condition showed that values of R_Ω increased significantly with increasing redox cycles, while values of the polarization resistance only increased slightly [16]. These previous results suggested that under the OCV condition only values of R_Ω were sensitive to the effect of redox. Though much has been learned on the redox of anode-supported button cells without interconnects under the OCV condition using EIS models and measurements [14–16], still little is known concerning variations of R_Ω and R_P for even a single-cell stack with interconnects under loaded conditions. Therefore, the key objective of this study is to measure and compare variations of R_Ω and R_P with the cell voltages under both unloaded and loaded conditions for the aforementioned two sets of nearly identical single-cell stacks except using different flow distributors via the EIS diagnosis.

The following section describes experimental methods and arrangements used in the study, including (1) a brief description of the test rig and the arrangement of anode and cathode connecting wires to the EIS measuring device, (2) measurements of electrochemical impedance spectra, and (3) measurements of SEM microstructure images for both anode and cathode surfaces of the PEN after 100 h of operation. Both impedance spectra data and SEM microstructures are then used to address effects of flow uniformity in interconnects on the performance and the anodic degradation of the single-cell stacks. We shall show that the re-oxidation behaviors in anode observed only in the case without using guide vanes are due to non-uniform flow distributions in interconnects. Finally, an equivalence circuit model is proposed in attempt to interpret these impedance data.

2. Experimental methods

2.1. Single-cell stack test using two different flow distributors

A SOFC testing platform was recently developed to measure the power-generating characteristics of the single-cell stack having flow distributors in both anode and cathode, as described in [2]. For completeness, a brief description of the test rig is given together with new modifications for EIS measurements. The left part of Fig. 1 presents a photograph showing the arrangement of the testing single-cell stack which is embedded in a ceramic housing inside a temperature-controlled furnace, whereas the middle part of Fig. 1 is an exploding sketch of such single-cell stack along with anodic and cathodic connecting wires to the EIS measuring devices on the right part of Fig. 1. The vertical tubular furnace (Fig. 1) can be used to heat up the single-cell stack from the room temperature to an operating temperature up to 1000 °C. In this study, the single-cell stack test is performed at a fixed temperature of $T = 850$ °C. Same as our previous study [2], we use the commercial anode-supported PEN (ASC 3 purchased from H.C. Starck) to perform the present power and impedance measurements. The structure and compositions of the PEN (ASC 3) are consisted of an anode support layer of NiO–YSZ (Yttria-stabilized Zirconia; Y_2O_2 doped with ZrO_2), an anode functional layer of NiO–YSZ, the electrolyte of YSZ, and a cathode functional layer of YSZ–LSM/LSM (Lanthanum Strontium Manganese oxide, $La_{0.65}Sr_{0.3}Mn_{1.0}O_3$; double layer). Therefore, the single cell is assembled by the aforementioned commercial anode-supported PEN (ASC 3) with a reactive area of 40 mm × 40 mm which is 16 times larger than that of commonly used button cells, a crofer 22-APU supporting frame, and two current collectors using a porous nickel sponge on the anode side and a platinum mesh on the cathode side for the collection of the electrode current. Then the PEN, the metallic frame, and the current collectors are sand-

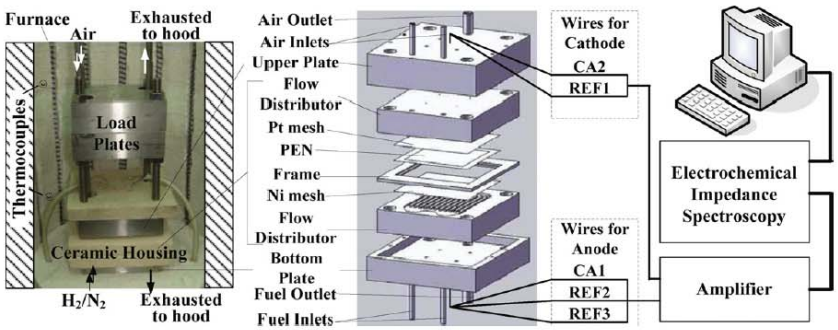

Fig. 1. Photograph of the test rig inside a furnace (left) and the exploding sketch of a single-cell stack using rib-channel flow distributors (middle) in both anode and cathode along with connecting wires to the EIS measuring devices (right).

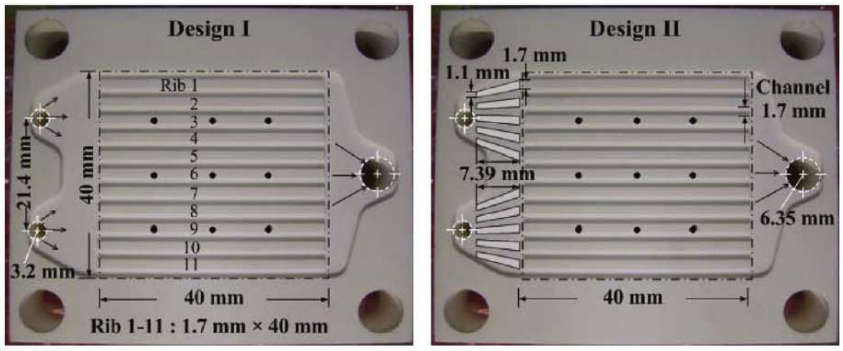

(a) Two different flow distributors

(b) PEN and frame

Fig. 2. (a) Two flow distributors, designs I and II, having the same double-inlet/single-outlet rib-channels, but only the design II using 10 small guide vanes equally positioned around the feed header, where precise dimensions of 11 equal-size ribs, 12 equal-size channels, feed header, and guide vanes are also indicated. Each of 12 channels and/or 11 ribs has 0.7 mm width and 40 mm long. (b) Photographs showing both anode and cathode sides of the PEN with crofer 22 frames before operation, where the white square strips on the cathode side are ceramic sealants to prevent any possible gas leakage at the frame.

wiched by the upper and lower flow distributors (please see both Figs. 1 and 2a) to form a single-cell stack. Note that the use of the metallic frame is to provide the mechanical support to the PEN and further prevent the possible cross-leakages between fuel and oxidant from both feed and exhaust headers of flow distributors. Both flow distributors, designs I and II as indicated in Fig. 2a without and with guide vanes, have nine small holes on their rib-channel area allowing the access of the voltage and current probes for measurements. For the sake of safety, several flame arresters are used and installed along the hydrogen supplied lines and cylinders. Also, the hydrogen gas detectors with the alarm system are also applied near the furnace to monitor possible hydrogen leakages. During the test, the exit gases from the single-cell stack are exhausted by a specially designed hood to the atmosphere after diluting with additional air.

In order to avoid the poisoning problem of the electrodes due to the chromium (Cr) volatilization from the metallic flow distributors at high-temperature conditions [17], we fabricate both anodic and cathodic flow distributors using aluminum oxide materials. As shown in Fig. 2a, two different flow distributors, designs I and II, are used in this study. Both designs have the same double-inlet/single-outlet rib-channels, but only the design II applies 10 small guide vanes equally positioned around the feed header (Fig. 2a) which can effectively improve the flow uniformity in flow distributors to be much better than that of design I. Same as [2], this study also applies 3-kg loading plates (see the left part of Fig. 1) to achieve a good electrical contact among the PEN and the two current collectors. In addition, the present single-cell stack is not tightly screwed having a seal-less assembly, so that the coefficient of thermal expansion (CTE) matching problem among different components of the single-cell stack can be eliminated [18]. It should be noted that by applying such seal-less assembly, one should avoid the cross-leakages of fuel and air in the single-cell stack that can result in serious cell degradation. Hence, two important things must be arranged. First, ceramic sealants must be carefully applied on the crofer 22-APU supporting frame for both anode and cathode sides to prevent any possible gas leakage at the frame, as can be clearly seen from Fig. 2b where the white square strips are ceramic sealants. Secondly, the flow rate of the anode must be kept equal to or slightly higher than that of the cathode in order to make sure no air leakage to the anode. In the present study, the flow rates of both anode and cathode sides for all experiments are kept the same ($Q_{H_2} = Q_{AIR} = 1$ slpm). Since both the mismatch of CTE among components and the Cr-poisoning problems can lead to rapid cell degradation [19], the above arrangements are essential to circumvent these complex problems. Thus, a clear-cut result concerning the impact of flow distributors on the performance and the anodic degradation of single-cell stacks can be obtained.

2.2. Testing procedures and impedance measurements

Since the standardization of the testing procedure is essential in order to obtain repeatable and reliable experimental data [20,21], we apply the same testing procedure proposed by Haanappel and Smith [20] for the present cell performance and impedance spectra measurements. A high reduction temperature at $T = 850\,^{\circ}C$ during the 24-h anode reduction process to achieve a higher cell performance is also applied in the present study. These measurements can be divided by three time stages. The first stage is the 24-h anode reduction period starting when $T = 850\,^{\circ}C$, where the flow rates in anode and cathode are, respectively, $Q_{anode} = 280\,cm^3\,min^{-1}$ ($80\,cm^3\,min^{-1}$ of $H_2 + 200\,cm^3\,min^{-1}$ of N_2) and $Q_{cathode} = 80\,cm^3\,min^{-1}$ of Air. After the completion of the anode reduction, Q_{anode} and $Q_{cathode}$ are very slowly modulated to the designed flow rates of $Q_{anode} = Q_{cathode} = 1000\,cm^3\,min^{-1}$, with an increment of no more than $100\,cm^3\,min^{-1}$, anode first and cathode, and then waiting for 30 min before the next increment to avoid any possible cell damage from a too-large-variation of flow rates and thus cell temperature. This process takes about 6 h, because the anode has 12 increments including 9 times of $100\,cm^3\,min^{-1}$ increment, 1 time of $20\,cm^3\,min^{-1}$ increment and the final 2 times of $100\,cm^3\,min^{-1}$ N_2 decrement, while the cathode has 10 times increments (9 times of $100\,cm^3\,min^{-1}$ increment plus 1 time of $20\,cm^3\,min^{-1}$ increment). The second is the data taking period, where the flow rate in anode is always kept equal to that of the cathode. This data taking process takes about 1 h starting from the OCV condition to various loaded conditions, with an increment of 0.2 A ($0.0125\,A\,cm^{-2}$). Each data point takes about 1 min to measure via the time average procedure. Finally, the third stage is to let the cell operate at a fixed voltage of 0.7 V for 100 h operation. For detailed descriptions on the start-up procedure, the reader is directed to [2].

The impedance spectra of two sets of nearly identical single-cell stacks are measured by the AC impedance analyzer (Bio-Logic, model SP-150) together with a current amplifier (Biologic, VMP3) to extend the measuring range of the operating current from ±800 mA to ±10 A. However, it is rather difficult to employ a reference electrode on the present square-shape large PEN, so that we apply the two-electrode system for EIS measurements. In other words, both the counter electrode and the reference electrode from the current amplifier and the EIS device are connected with the current collector in the cathode side of the single-cell stack. As schematically sketched on the right part of Fig. 1, the positive electrode (cathode) of the single-cell stack is connected to REF1 + CA2, while the negative electrode (anode) is connected to REF2 + REF3 + CA1. Note that CA1 and CA2 represent, respectively, the current control and measurement through the working and the counter electrodes, and REFs 1, 2 and 3 indicate the control and measurement of the working electrode potential, the reference electrode potential and the counter electrode potential, respectively. Fig. 3 shows schematics and descriptions of various probes (REFs 1, 2, 3 and CAs 1, 2) for EIS measurements, where eight wires equally spaced on both anode and cathode surfaces are used to collect uniformly and effectively the impedance data from the anode-supported single-cell (ASC-3 purchased from H.C. Starck). Using an AC sinusoidal-wave potential perturbation with signal amplitude of 20 mV, the AC impedance of the single-cell stacks can be obtained by measuring the corresponding current response. In the present study, the impedance measurements are carried out at various DC conditions varying from OCV to 0.6 V, each condition covering a range of frequency from 50 mHz to 3 kHz, so that several overlapping responses due to various mechanisms, such as kinetics of electrochemical reactions and diffusions, may be analyzed under different DC loads.

To clearly show how ohmic and polarization resistances are determined from the Nyquist plot, Fig. 4a presents a typical measured impedance spectrum using the design II operated at the OCV condition. In it values of R_Ω and R_P are multiplied by the effective anodic reactive surface area A_{eff} (=16 cm^2) as indicated by RA_Ω and RA_P in Fig. 4a that can be determined from the intersecting points on the real axis of the Nyquist plot. Then the total impedance is the sum of RA_Ω and RA_P. As can be seen, these data points in Fig. 4a can be well represented by a fitting curve derived from an appropriate equivalent circuit model (ECM), as to be discussed in the next subsection. By directly comparing the electrochemical impedance spectra data between these two nearly identical single-cell stacks except using different designs of flow distributors, we should be able to address the question on why the better flow uniformity in interconnects can effectively improve the cell power density.

2.3. Equivalent circuit model

Because the physical and chemical processes of electrochemical devices are usually very complex and non-linear, there is a need

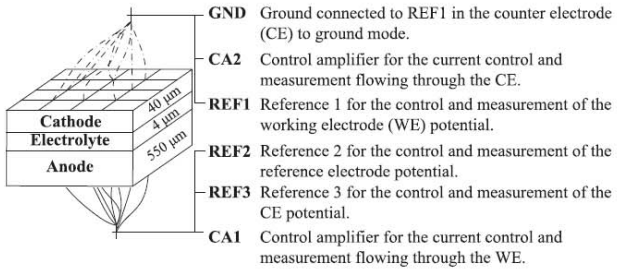

Fig. 3. Schematics of various probes for EIS measurements with detailed descriptions, where eight wires equally spaced on both anode and cathode surfaces are used to collect uniformly and effectively the impedance data from the anode-supported single-cell (ASC-3 purchased from H.C. Starck).

to further develop an appropriate ECM that may be used to fit the experimental impedance data and thus explain some impedance characteristics of the electrochemical devices [11,12]. Fig. 4b shows a typical ECM for the total impedance that often consists of a number of basic lumped elements of the inductors (L), the capacitors (Q), and the resistors (R) in series or in parallel and/or in a combination of both. The corresponding mathematic expression of the total impedance for the present single-cell stacks may be represented by $Z(i\omega) = Z_L + Z_R + Z_{RQ1} + Z_{RQ2} + Z_{RQ3}$, where the induction impedance $Z_L = i\omega L$ is due to the device's electromagnetic induction, the ohmic impedance $Z_R = R_\Omega$ is contributed by ions/electrons transferring in the electrolyte/conductor, and $Z_{RQj} = R_j/[(i\omega)^{nj} R_j Q_j + 1]$ with the subscript $j = 1, 2, 3$ indicating various contributions from such as the electrodes' porosity, non-uniform distribution of reaction rates, and surface roughness and compositions [9,10]. Values of Z_R ($=R_\Omega$) are real in the complex plane that are independent of frequency and can be determined from the intersecting point along the real axis on the Nyquist plot. On the other hand, the frequency-dependent elements, Z_L and $(i\omega)^{-n}Q^{-1} = Z_P$, have only the imaginary contribution and thus their impedance spectra should be parallel to the imaginary axis [5–7]. Note that Z_P is a basic element, also known as the constant-phase element (CPE) which is commonly used in the ECM for fuel cells. For the present single-cell stacks, three CPEs are applied as indicated by CPE_1, CPE_2 and CPE_3 in Fig. 4b, corresponding to three overlapping arcs or semicircles with their centers positioned at the real axis (Fig. 4a). In this work, the proposed ECM, as shown in Fig. 4b, is used in attempt to explain these measured impedance data.

3. Results and discussion

3.1. Power-generating characteristics and anodic re-oxidation observation

Before presenting the AC impedance spectra, we first present the comparison of power generating characteristics between the two sets of nearly identical single-cell stacks except using different flow distributors (designs I and II) as shown in Fig. 5. In it values of the power density for both cases quickly increase from zero to 281 mW cm^{-2} for the design I and/or 322 mW cm^{-2} for the design II, as values of the current density I_d increase from zero to 400 mA cm^{-2} under loaded conditions. There is a 12.5% increase in the value of the power density for the design II using guide vanes as compared to that of the design I without using guide vanes at the same $I_d = 400$ mA cm^{-2}, indicating an important point that the higher flow uniformity in flow distributors is, the better cell performance is. Due to very high flow rates ($Q_{H_2} = Q_{AIR} = 60\,l\,h^{-1}$) used in the present study, the fuel and air utilization rates are rather small. Note that the fuel and/or utilization rates can be estimated using the ratio of the effective usage of H_2 and/or air flow rates ($Q_{H_2,eff}$ and/or $Q_{AIR,eff}$) for power generation to the total supply of H_2 and/or air flow rates ($Q_{H_2,total}$ and/or $Q_{AIR,total}$). $Q_{H_2,eff} = nI/2F$ (moles s^{-1}) and $Q_{AIR,eff} = nI/4F$ (moles s^{-1}), where n is the cell number, F is the Faraday constant (=96485 C mole^{-1}), and I is the current. In the present study, $n = 1$, $I_{max} = 6.4$ A (or 400 mA cm^{-2} in current density) for both cases in Fig. 5 to avoid the occurrence of the concentration

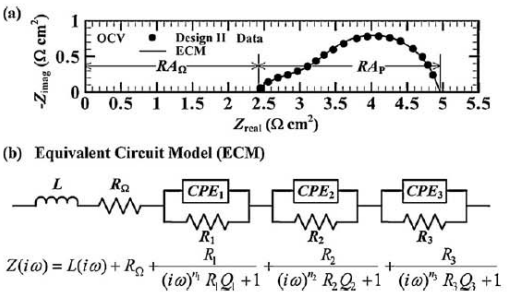

Fig. 4. (a) A typical impedance spectrum obtained at the OCV condition using the design II interconnects with small guide vanes showing the determination of ohmic and polarization impedances (RA_Ω and RA_P). The solid points are the measured impedance data and their fitting line is via the equivalent circuit model as shown in (b) which is used to fit and explain the impedance data of the present single-cell stacks using different designs of flow distributors.

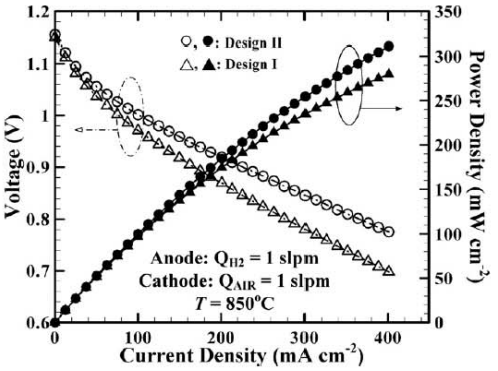

Fig. 5. Comparison of power-generating characteristics between two sets of the single-cell stack under the same experimental conditions except using different designs of flow distributors.

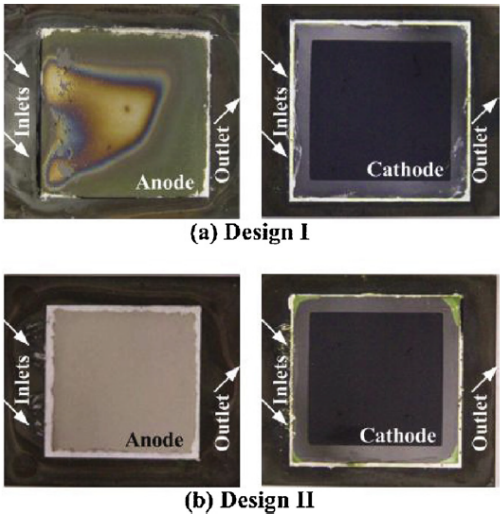

Fig. 6. Photographs of both anode and cathode surfaces of the PEN after 100 h of operation using different designs of flow distributors: (a) Design I and (b) Design II, in which the design I case has severe anodic re-oxidation zones while the design II case using small guide vanes having much better flow uniformity in flow distributors is free from any anodic re-oxidation.

polarization at higher loads, and $Q_{H_2,total} = Q_{AIR,total} = 1\,l\,min^{-1}$, so that the fuel utilization rate is 4.8% and the air utilization rate is 1.2%.

Fig. 6a and b presents photographs of the anode and the cathode surfaces of the PEN after 100 h of operation for both designs using two different flow distributors, respectively, (a) design I and (b) design II. As can be seen from Fig. 6b, no anodic re-oxidation can be observed in the case of the design II using simple guide vanes having excellent flow uniformity in flow distributors, where the anodic surface still remains a fully reduced metallic Ni/YSZ surface with uniform grey color even after 100 h of the continuous cell operation. On the other hand, under the same experimental conditions, severe anodic re-oxidation zones ($Ni_{1-\delta}O$/YSZ) are observed in the case of design I without using guide vanes having not-so-good flow uniformity in flow distributors, where the anodic catalyst changes colors from green to dark green and/or black with increasing δ (Fig. 6a). Since the same flow rates are carefully applied to both the anode and the cathode ($Q_{H_2} = Q_{AIR} = 1$ slpm) in the present study to avoid any possible air leakage to the anode, the anodic re-oxidation observed only in the case of design I is thus due to non-uniform flow distributions in interconnects. It is thought that the smaller fuel flow velocities in some of 12 flow rib-channels (design I) can lead to higher fuel utilization. This may further cause a significant drop of the fuel partial pressure (close to zero), the so-called fuel starvation, that can occur locally for some very small fuel flow velocities, eventually resulting in the occurrence of the locally anodic re-oxidation in the case of design I (see Fig. 6a). Note that the anodic re-oxidation can decrease the porosity of the anode which in turn limits the fuel diffusion process and may cause micro cracks at the interface between the anode and the electrolyte. As to the cathode surfaces, both cases (designs I and II) look almost the same even after 100 h of operation (Fig. 6a and b). This is probably because the cathode has much slower reaction rates of oxygen. Hence, these results indicate that the unwanted local re-oxidation of the anode after long time cell operation can be avoided

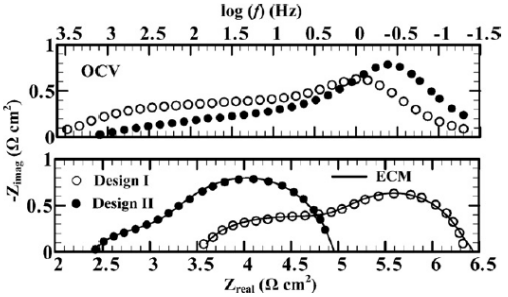

Fig. 7. The Nyquist plot of the two sets of nearly identical single-cell stacks except that the feed headers of the rib-channel flow distributors were different, one with small guide vanes that can significantly increase flow uniformity (design II) and the other without (design I), in which data are measured at the OCV condition over a wide frequency range from 50 mHz to 3 kHz while keeping all operating conditions the same for both cases.

by improving the degree of flow uniformity in flow distributors and thus the longevity of the cell stack may be extended.

It should be noted that the difference of the data between designs I and II (about 12% differences in power density) is not due to the gas-leakage because of the following four reasons. (1) There is no gas-leakage at the frame, because we have carefully applied ceramic sealants on the crofer 22-APU supporting frame for both anode and cathode sides to fix the PEN and to prevent any possible gas leakage at the frame (see Fig. 2b). (2) There is no air leakage to the anode, since we have carefully controlled the flow rate in anode to be at least equal to or higher than that of the cathode. In addition, the present study applies high flow rates (60 l h^{-1} and/or 1 slpm controlled by precision flow meters) in both anode and cathode to provide sufficient gases in the single-cell stack and thus make sure no gas-leakage from the outside furnace environment into the cell. (3) With a 3-kg load applied for achieving a good contact of current collectors, the amount of gas-leakage from the cell to the furnace is very small having little influence on the cell performance especially in the high-temperature furnace environment where $T = 850\,^{\circ}C$. (4) The present results are not obtained from just one-shot experiment, because we have repeated the same experiments for at least three times to confirm the repeatability of these results. Furthermore, the degradation of cell performance is less than 1% after the long time (100 h) operation showing that the PENs have absolutely no cracks at all. Note that the crack of the PENs is the only possible way for the gas-leakage and this does not occur in the present study. Hence, by comparing two sets of nearly identical single-cell stacks under exactly the same experimental conditions except that different designs of flow distributors (designs I and II) are used, we are able to obtain a clear-cut result on the impact of flow distributors to cell performance and impedance spectra when the above arrangements are applied.

3.2. AC impedance spectra at open-circuit voltage and loaded conditions

At the same OCV condition, Fig. 7 presents the comparison of the impedance spectra including both the Bode plot (top) and the Nyquist plot between the two sets of nearly identical single-cell stacks except using different flow distributors (designs I and II), in which the same experimental conditions, e.g., $T = 850\,^{\circ}C$ and $\dot{Q}_{H_2} = \dot{Q}_{AIR} = 1000$ ml min^{-1}, are applied. These measured impedance data points, as indicated by the circle symbols scanning from ~0 Hz on the right end to the highest frequency (~3 kHz) on the left end in Fig. 7, can be well fitted by the proposed ECM (see Fig. 4b) rep-

Table 1
Comparisons between designs I and II for various key elements in the proposed equivalent circuit model as shown in Fig. 4b.

ECM elements	OCV		1 V		0.8 V		0.6 V	
	I	II	I	II	I	II	I	II
L (μH)	0.494	0.512	0.486	0.504	0.492	0.51	0.496	0.509
R_Ω (Ω)	0.219	0.149	0.221	0.151	0.218	0.150	0.218	0.150
Q_1 (Fs^{n_1-1})	0.019	0.062	0.033	0.105	0.04	0.167	0.048	0.403
n_1	0.855	0.842	0.762	0.79	0.747	0.781	0.736	0.739
R_1 (Ω)	0.031	0.012	0.039	0.01	0.033	0.006	0.032	0.004
Q_2 (Fs^{n_2-1})	0.632	1.46	0.635	1.782	0.713	1.731	0.84	1.788
n_2	0.601	0.605	0.643	0.625	0.645	0.643	0.652	0.634
R_2 (Ω)	0.092	0.053	0.064	0.036	0.054	0.023	0.049	0.021
Q_3 (Fs^{n_3-1})	3.645	4.449	3.664	6.033	5.395	9.331	9.797	12.92
n_3	1	0.931	0.954	0.997	0.946	0.911	0.988	0.918
R_3 (Ω)	0.059	0.099	0.045	0.04	0.021	0.019	0.01	0.01

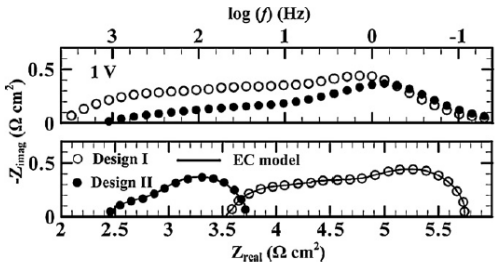

Fig. 8. Same as Fig. 7, but data are measured at the loaded condition when the single-cell stacks are operated at 1 V.

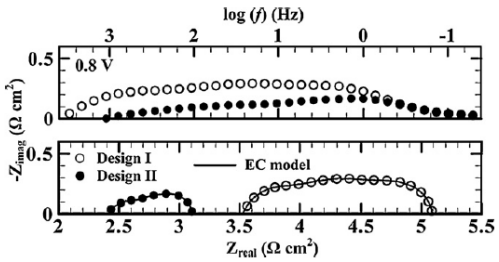

Fig. 9. Same as Fig. 7, but data are measured at 0.8 V.

resented by the solid line on the Nyquist plot. As mentioned in the previous section, the present ECM includes three CPEi (i = 1, 2, 3) corresponding to three overlapping arcs or semicircles, each CPE representing a physical or chemical process. Note that there are

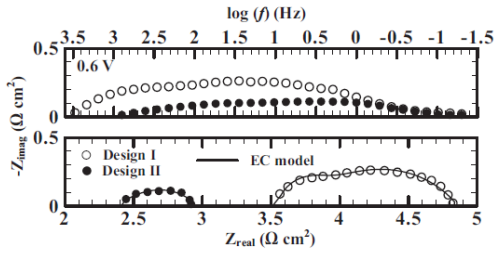

Fig. 10. Same as Fig. 7, but data are measured at 0.6 V.

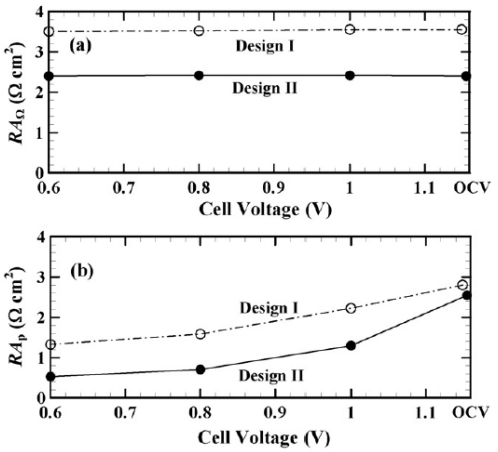

Fig. 11. (a) Comparison of the ohmic resistance between the two sets of nearly identical single-cell stacks using different designs of flow distributors (designs I and II) plotted against different cell voltages varying from OCV to 0.6 V. (b) Same as (a), but for the polarization resistance data.

two intersecting points by the proposed model line on the Z_{real} axis of the Nyquist plot, at which the two corresponding values of Z_{real} are used to determine values of RA_Ω and RA_P (see also Fig. 4a). It is found that $RA_\Omega \approx 3.50\,\Omega\,cm^2$ and $RA_P \approx 2.80\,\Omega\,cm^2$ for the design I without using guide vanes having a total impedance value of $RA_{tot} = RA_\Omega + RA_P \approx 6.30\,\Omega\,cm^2$, while smaller values of $RA_\Omega \approx 2.40\,\Omega\,cm^2$ and $RA_P \approx 2.54\,\Omega\,cm^2$ are found for the design II using guide vanes with $RA_{tot} \approx 4.94\,\Omega\,cm^2$ which is 22% lower than that of the design I (see also Table 1). At the OCV condition, the design I case without using guide vanes having not-so-good flow uniformity in interconnects suffers a larger value of RA_Ω which is 32% higher than that of the design II case. Clearly, this is because the latter case uses simple guide vanes equally spaced around the feed header of rib-channel flow distributors, so that an excellent flow uniformity in flow distributors can be achieved and thus a lower value of impedance is found. As to the polarization resistance, a more modest influence of flow uniformity is found at the OCV condition, where the value of RA_P for the design I case is only 9% higher than that of the design II case. These results measured at the OCV condition seem to be consistent with previous results [16] in which the value of RA_Ω was found to be more sensitive to the effect of redox than the value of RA_P. Therefore, the improvement of flow uniformity in flow distributors is useful to decrease both values of RA_Ω and RA_P of single-cell stacks, in

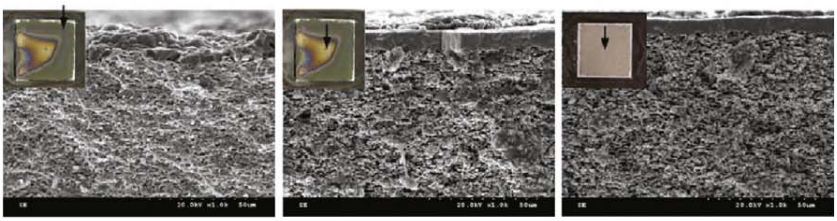

Fig. 12. Comparisons of SEM images showing different anodic microstructures of the PEN after 100 h of operation when two different designs of flow distributors with different degrees of flow uniformity are used.

particular for the decrease of the ohmic resistance when the OCV condition is considered.

Same as Fig. 7 but measured at loaded conditions, Figs. 8–10 show the comparison of the impedance spectra between designs I and II at 1 V, 0.8 V and 0.6 V, respectively. It is found that values of RA_{Ω} for both cases measured at various loaded conditions remain essentially the same as that measured at the OCV condition. In other words, the ohmic resistance does not vary with the loaded cell voltage. This can be more easily from Fig. 11a, where values of RA_{Ω} for both cases are plotted against the cell voltage. Furthermore, the better flow uniformity in interconnects is, the lower values of RA_{Ω} are. As to values of RA_P as a function of the cell voltage, a totally different trend is found. Values of RA_P for both designs decrease with decreasing the cell voltage, as can be clearly seen in Fig. 11b. This is because decreasing the cell voltage and/or increasing the loaded current can result in more active electrochemical reactions and thus reduce values of RA_P. In addition, the percentage differences in values of RA_P between designs I and II, defined as $(RA_{P,I} - RA_{P,II})/RA_{P,I}$, increase as the cell voltage decreases, which are, respectively, from 9% at OCV to 42% at 1 V, 56% at 0.8 V and 60% at 0.6 V (see Fig. 11b). The higher values of RA_P found in the design I case as compared to that of the design II case are again attributed to the locally anodic re-oxidation occurring only in the design I case. As pointed out by Pihlatie et al. [22], the anodic porosity can be significantly decreased by the oxidation of Ni to NiO due to the volume increase of NiO which is 69% more in volume than Ni. Consequently, for the design I case, the diffusion processes of hydrogen fuel and steam in anode are depressed, resulting in a decrease of available three-phase boundary length and thus an increase in values of RA_P.

Concerning the Bode plots on the top of Figs. 7–10, it provides the frequency information of the present impedance data including three summit frequencies (f_{summit}) that correspond to the last three terms (Z_{RQ1}, Z_{RQ2}, Z_{RQ3}) or three overlapping arcs in the proposed ECM (see Fig. 4b and Table 1) as also plotted in the Nyquist plot. Each of them may reflect a physical or chemical process with reference to Laurencin et al. [16]. For Z_{RQ1} at the high frequency range in the model (Fig. 4b), $f_{summit,1}$ = 954–1139 Hz (design I) and 827–1101 Hz (design II) that may be related to anodic chemical reaction processes [16]. For Z_{RQ2} at the middle frequency range, $f_{summit,2}$ = 18–25 Hz (design I) and 11–28 Hz (design II) that may be dominated by gas diffusion processes near the electrode structure [16]. For Z_{RQ3} at the low frequency range, $f_{summit,3}$ = 0.7–1.7 Hz (design I) and 0.4–1.5 Hz (design II) that may be influenced by electrochemical reaction processes in the cathode [16]. However, it is far beyond the scope of the present study to identify actually how many physically relevant processes the impedance of the single-cell stack includes. This is because the impedance of the single-cell stack is very complex that may involve many physical and chemical processes. Therefore, these three overlapping arcs ($Z_{RQ1} + Z_{RQ2} + Z_{RQ3}$) corresponding to three summit frequencies reflecting different physical processes in the proposed model (Fig. 4b) should be viewed with some caution due to the limited numbers of impedance experiments conducted. Nevertheless, the present impedance data and their associated discussion do provide a clear-cut result based on values of RA_{Ω} and RA_P that can be used to explain why by improving flow uniformity in interconnects can effectively reduce the impedance and thus increase the cell performance of the single-cell stack.

3.3. Anodic microstructure analysis by SEM

Fig. 12 presents comparisons of SEM images showing three different anodic microstructures of the PEN when using two different designs of flow distributors (designs I and II), respectively, (a) the design I case taken from the anodic re-oxidation zone (NiO), (b) the design I case taken from the still Ni catalyst region, and (c) the design II case without the occurrence of re-oxidation (Ni). Note that the annexes on the top left of these SEM images with the arrows show the locations where the samples are taken from. It can be directly seen from Fig. 12a that the occurrence of the unwanted re-oxidation zone on the anodic surface can significantly reduce the porosity of the anode. This in turn depresses the fuel diffusion process through the porous anode possibly making micro cracks at the interface between the anode and the electrolyte and eventually causing the sever degradation of the anodic catalyst. In addition, when the local re-oxidation of the anode occurs, the corresponding location of the Ni-mesh is also oxidized, further inhibiting the pass way of the electrons from the anode to the current collector and thus resulting in an increase of the impedance. On the other hand, when the design II with a very high degree of flow uniformity in flow distributors is applied, the anodic Ni catalyst can be free from the re-oxidation (Fig. 12c). Hence, the improvement of flow uniformity in flow distributors not only can avoid the unwanted local re-oxidation of the anode but also can reduce the impedance, showing the important impact of flow distributors on the performance and the longevity of the cell stack.

4. Conclusions

A clear-cut result concerning the impact of flow distributors on the electrochemical impedance of single-cell stacks is presented. This is achieved by comparing the impedance spectra between two sets of nearly identical single-cell stacks measured by the electrochemical impedance spectroscopy under the open-circuit voltage and at various loaded conditions, where all experimental procedures and conditions are kept the same except using different flow distributors (designs I and II) in these two stacks. Results show that the ohmic resistance for both designs is independent of the cell voltage where values of RA_{Ω} at various loaded conditions are essen-

tially the same as that obtained at the OCV condition, while the polarization resistance is sensitive to the cell voltage where values of RA_P decrease with decreasing the cell voltage (Fig. 11). The latter is because increasing the loaded current and/or decreasing the cell voltage can result in more active electrochemical reactions. As to the impact of flow distributors, the better flow uniformity in flow distributor is, the lower values of RA_Ω and RA_P are. When compared at the same operating conditions (0.6 V at 850 °C), it is found that both values of ohmic and polarization resistances of the single-cell stack using guide vanes having excellent flow uniformity in interconnects are, respectively, 32% and 60% smaller than that without using guide vanes having not-so-good flow uniformity in interconnects. These results explain why the power density of the present single-cell stack can be increased more than 10% by just improving flow uniformity in interconnects (Fig. 5). Moreover, the higher values of RA_Ω and RA_P found in the design I case as compared to that of the design II case are attributed to the locally anodic re-oxidation occurring only in the design I case due to non-uniform flow distributions in interconnects, as also confirmed by SEM microstructure observations (Fig. 12). It is thus concluded that the improvement of flow uniformity in flow distributors not only can reduce the impedance of the cell stack but also can avoid the unwanted local re-oxidation of the anode. As such, the present measurements are useful for further improving the performance and the longevity of planar SOFCs.

As a final remark, we are currently conducting high-pressure experiments in a newly established double-chamber SOFC testing facility. Power generating characteristics and impedance spectra for single-cell stacks using different designs of flow distributors at elevated pressures up to 5 atm will be measured, aiming to provide the basic knowledge for the future development of the high-efficiency SOFC and gas turbine integrating power generation technology. These results will be published in the near future.

Acknowledgments

The authors would like to thank the referees for their valuable comments. This work was continuously supported by the Institute of Nuclear Energy Research (972001INER036, 982001INER040, and 992001INER048) and the National Science Council (NSC97-2212-E-008-085-MY3, 98-2221-E-008-058-MY3, and 98-3114-E-008-004) in Taiwan.

References

[1] C.M. Huang, S.S. Shy, C.H. Lee, J. Power Sources 183 (2008) 205–213.
[2] C.M. Huang, S.S. Shy, H.H. Li, C.H. Lee, J. Power Sources 195 (2010) 6280–6286.
[3] H. Yakabe, Y. Baba, T. Sakurai, M. Satoh, I. Hirosawa, Y. Yoda, J. Power Sources 131 (2004) 278–284.
[4] H. Yoshida, H. Yakabe, K. Ogasawara, T. Sakurai, J. Power Sources 157 (2006) 775–781.
[5] J.R. Macdonald, J. Appl. Phys. 58 (1985) 1971–1978.
[6] J.R. Macdonald, J. Appl. Phys. 61 (1987) 700–713.
[7] J.R. Macdonald, J. Appl. Phys. 65 (1989) 4845–4853.
[8] C.A. Schiller, W. Strunz, Electrochim. Acta 46 (2001) 3619–3625.
[9] C.H. Kim, S.L. Pyun, J.H. Kim, Electrochim. Acta 48 (2003) 3455–3463.
[10] J.B. Jorcin, M.E. Orazem, N. Pébère, B. Tribollet, Electrochim. Acta 51 (2006) 1473–1479.
[11] E. Barsoukov, J.R. Macdonald, Impedance Spectroscopy Theory, Experiment, and Applications, 2nd ed., John Wiley & Sons, Inc., New Jersey, 2005.
[12] Q.A. Huang, R. Hui, B. Wang, J. Zhang, Electrochim. Acta 52 (2007) 8144–8164.
[13] M. Gong, X. Liu, J. Trembly, G. Johnson, J. Power Sources 168 (2007) 289–298.
[14] B. Iwanschitz, J. Sfeir, A. Mai, M. Schütze, J. Electrochem. Soc. 157 (2) (2010) B269–B278.
[15] B. Liu, Y. Zhang, B. Tu, Y. Dong, M. Cheng, J. Power Sources 165 (2007) 114–119.
[16] J. Laurencin, G. Delette, B. Morel, F. Lefebvre-Joud, M. Dupeux, J. Power Sources 192 (2009) 344–352.
[17] K. Hilpert, D. Das, M. Miller, D.H. Peck, R. Weiβ, J. Electrochem. Soc. 143 (1996) 3642–3647.
[18] H.C. Liu, C.H. Lee, Y.H. Shiu, R.Y. Lee, W.M. Yan, J. Power Sources 167 (2007) 406–412.
[19] H. Tu, U. Stimming, J. Power Sources 127 (2004) 284–293.
[20] V.A.C. Haanappel, M.J. Smith, J. Power Sources 171 (2007) 169–178.
[21] V.A.C. Haanappel, A. Mai, J. Mertens, Solid State Ionics 177 (2006) 2033–2037.
[22] M. Pihlatie, A. Kaiser, M. Mogensen, Solid State Ionics 180 (2009) 1100–1112.